International Journal of Earth Sciences (2021) 110:2863–2884
https://doi.org/10.1007/s00531-021-02088-8

ORIGINAL PAPER

Origin and evolution of the Oligocene rhyolitic magmas in the Mesa Central of Mexico: geochemical, petrological and geochronological evidence from the Guanamé Ignimbrite

Pascal Sieck[1] · Rubén Alfonso López-Doncel[1] · Alfredo Aguillón-Robles[1] · Jorge Uriel Cruz-Castillo[2] · Klaus Wemmer[3]

Received: 1 April 2020 / Accepted: 30 June 2021 / Published online: 12 July 2021

Abstract
Oligocene explosive volcanism is widespread in the central and eastern portion of the Mesa Central (MC), but the origin of the rhyolitic magmas is still under discussion. The Guanamé Ignimbrite is located in the northern portion of the Salinas-Villa de Ramos volcanic field (SVRVF) and a typical rhyolitic and porphyric Oligocene ignimbrite in the central and eastern portion of the MC. U–Pb zircon single grain age determination reveals a crystallization between 30.61 ± 0.73 Ma and 30.73 ± 0.39 Ma and an eruption at 30.12 ± 0.45 Ma (K–Ar whole rock). Chondrite-normalized rare-earth element patterns and primitive mantle-normalized multi-element patterns show enrichment in light rare-earth elements (LREE) and high field strength elements (HFSE). Geochemical features and mineral chemistry show that the rhyolitic magmas generated in an intra-plate and extensional setting from partial melting of the lower crust. During the ascent and storage in a shallow magma chamber, fractional crystallization of mainly plagioclase and oxides was the major process taking place in the evolution of the magma. Rhyolite-MELTS models reveal that these rhyolitic magmas were generated by partial melting of the well-studied lower crust in the MC. The models result in a similar mineral assemblage as observed in the samples. The mineral composition and crystallization temperatures of feldspars analyzed in this study are similar to the models confirming the lower crustal origin.

Keywords Rhyolitic ignimbrite · Sierra Madre Occidental · Mesa Central · Oligocene · Mexico

Introduction

The study area is located in the southeastern portion of the Mexican Sierra Madre Occidental (SMO), the Mesa Central physiographic province (MC). The SMO is dominated by large volumes of silicic volcanic rocks and the origin of this magmatic province has been associated to an extension of the continental crust, mainly in western Mexico (McDowell and Clabaugh 1979; Cameron and Hanson 1982; Swanson and McDowell 1984; Smith et al. 1996). The volcanism was effusive and explosive; however, part of the mainly Oligocene explosive volcanism is associated to the Ignimbrite Flare-Up, where ~ 400,000 km^3 of rhyolitic ignimbrites and rhyolites were erupted between 38 and 18 Ma, with two main peaks at ca. 34–28 Ma and ca. 24–18 Ma (Aguirre-Díaz and McDowell 1991; Ferrari et al. 2002; Bryan et al. 2008; Aguillón-Robles et al. 2009, 2014; Tristán-González et al. 2009a; Bryan and Ferrari 2013). In the southern Mesa Central, the volcanism is predominantly effusive (75%) and in less proportion explosive, mostly rhyolitic ignimbrites (Aguirre-Díaz et al. 2008; Aguillón-Robles et al. 2009). In the western and central portion of San Luis Potosí state, an extension of the SMO is composed of three volcanic fields that have been previously described. First, the San Luis Potosí volcanic field (SLPVF), which is formed by volcanic sequences of mainly felsic composition, erupted in 5 periods between 45 and 0.4 Ma (Labarthe-Hernández et al. 1982;

✉ Pascal Sieck
pascal.sieck@gmail.com

[1] Instituto de Geología, Universidad Autónoma de San Luis Potosí, Av. Dr. Manuel Nava 5, C.P. 78240 San Luis Potosí, México

[2] Area Ciencias de La Tierra, Facultad de Ingeniería, Universidad Autónoma de San Luis Potosí, Av. Dr. Manuel Nava 8, C.P. 78240 San Luis Potosí, México

[3] Geosciences Centre, Georg-August-Universität Göttingen, Goldschmidtstraße 3, 37077 Göttingen, Germany

Aguillón-Robles et al. 2009, 2012, 2014; Tristán-González et al. 2009a). Second, the Río Santa María volcanic field (RSMVF) that initiated with andesitic volcanism, which was followed by the emplacement of large volumes of rhyolitic pyroclastic flows, intercalated with andesitic and trachytic lava flows (Tristán-González et al. 2009a; Aguillón-Robles et al. 2012), and third, the Salinas-Villa de Ramos volcanic field (SVRVF) that is located along the limits of the states of San Luis Potosí and Zacatecas, in particular in the central portion of the MC (Tual 2010; Rodríguez-León 2012). In these three volcanic fields, the Ignimbrite Fare-Up initiated around 32 Ma in the SVRVF and the RSMVF (Tristán-González et al. 2009a; Sieck et al. 2019) and between 31 and 29 Ma in the SLPVF (Tristán-González et al. 2009a; González-Naranjo et al. 2012 and this study). The explosive volcanic activity lasted until 28–26 Ma and is dominated by rheomorphic ignimbrites (Labarthe-Hernández et al. 1982; Tristán-González et al. 2009a; González-Naranjo et al. 2012). As in many parts of the SMO and MC, calderas and caldera-like structures are not observable. The absence was interpreted as fissure-type volcanism along NW–SE trending faults and fissures (Aguirre-Díaz and Labarthe-Hernández 2003; Aguirre-Díaz et al. 2008; Tristán-González et al. 2008, 2009b; Sieck et al. 2021).

Studies on the origin of the rhyolitic magmas in the Mesa Central are rare and mainly from the last decades. Most works on the rhyolitic Oligocene rocks in the MC are restricted to general geochemical classifications without information regarding the genesis and evolution of the magmas. A first petrogenic study was carried out by Verma (1984) who concluded that the felsic domes in Zacatecas were derived from partial melting of the continental crust. The first detailed geochemical and petrological study to present a generalized model of the magmatic evolution in the Mesa Central was carried out by Orozco-Esquivel et al. (2002), resulting in a formation model including the generation of rhyolitic magmas by partial melting of the continental crust. Near the study area, Aguillón-Robles et al. (2009) presented a detailed model of the origin and evolution of the rhyolitic domes in the southern MC indicating an origin by partial melting of the base of the continental crust in an intra-plate setting, and fractional crystallization during magma ascent, but due to poor stratigraphic control in their study, it is not clear which volcanic unit corresponds to which magmatic process and also, they base their results on only a few geochemical analyses. Another proposal is that intermediate to felsic magma compositions are the product of fractional crystallization of mafic magmas associated to contamination of the lithospheric base and mingled with existing magmas and were extruded through regional falls and fissures associated with crustal extension with NW–SE main orientation (Aguillón-Robles et al. 1994, 2009; Aranda-Gómez et al. 2007; Tristán-González et al. 2009b). Newer investigations on the Oligocene rhyolitic rocks in the MC show that almandine-rich garnets crystallized at lower crustal depth from a rhyolitic magma (Sieck et al. 2019). On the other hand, Torres-Sánchez et al. (2019) report an upper crustal origin of Oligocene felsic volcanic rocks in the San Luis Potosi volcanic field. The composition and age of the lower continental crust and the upper mantle in the MC is well known from crustal and mantle xenoliths in the Quaternary volcanism and has been studied in detail by Schaaf et al. (1994). Similar crustal xenoliths are observed in different Oligocene units in the San Luis Potosí Volcanic Field about 40–50 km south of the study area, but they have not been studied. The Guanamé Ignimbrite is located in the northern portion of the SVRVF and had not been studied in detail yet. Nevertheless, the chemical composition and age, as well as the lack of a caldera or caldera-like structure of the Guanamé Ignimbrite, is comparable to many other ignimbrites in the central and western portion of the MC and the three volcanic fields in that area (e.g., Orozco-Esquivel et al. 2002; Sieck et al. 2019; Torres-Sánchez et al. 2019; present work).

In this work trace-element and geochronological data are used to reconstruct the magmatic evolution of the Guanamé Ignimbrite as an example for the origin of the rhyolitic volcanism in the central portion of the MC. In addition, the present work uses the geochemical and petrological data of the lower crustal xenoliths presented by Schaaf et al. (1994) to prove the lower crustal origin of the rhyolitic magmas that originated the explosive volcanism in the central and eastern part of the MC.

Geological framework and stratigraphy

Geological framework

Guanamé is located in the northern part of the SVRVF, in the central part of the Central Mexico Mesozoic Basin near the border of the Sierra Madre and the Guerrero Terranes (Fig. 1; Campa and Coney 1983) in the southeastern part of the MC. The Sierra Madre Terrane is built up by the Central Mexico Mesozoic Basin (CMMB) and the Valles-San Luis Potosí Platform (VSLPP). The CMMB, which forms the basement of the study area, is constituted by a marine Mesozoic sedimentary sequence of more than 5000 m in thickness, initiating in the late Triassic and culminating in the late Cretaceous (Carrillo-Bravo 1982). The VSLPP consists of Paleozoic and Precambrian metamorphic basement, unconformably overlain by Jurassic clastic sediments (Barboza-Gudiño et al. 2008). Precambrian and Jurassic rocks are overlain by a transgressive Cretaceous marine sequence that includes evaporites and shallow water limestones, recording a maximum water level during the Albian–Cenomanian

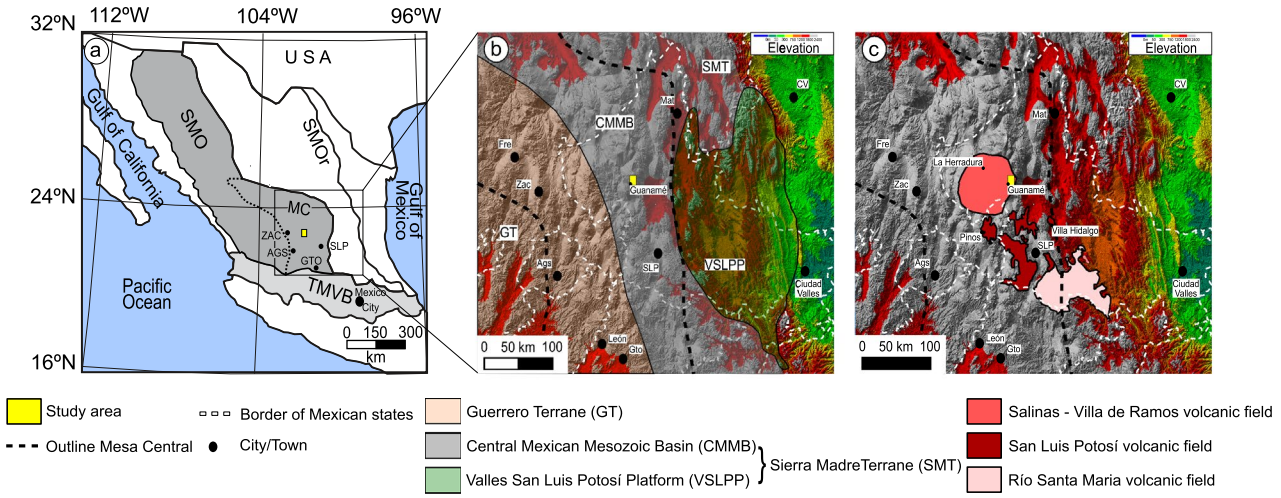

Fig. 1 Location of the study area. **a** Spatial relationship with the main geological provinces of northern Mexico. **b** Location of the Mesozoic volcano-tectonic features of the State of San Luis Potosí and Zacatecas. **a**, **b** modified after Aguillón-Robles et al. (2014). **c** Oligocene–Miocene volcanic fields in the central-eastern portion of the Mesa Central. *AGS* Aguascalientes city, *GTO* Guanajuato city, *SLP* San Luis Potosí city, *L* Leon, *ZAC* Zacatecas city, *CMMB* Central Mexico Mesozoic Basin, *GT* Guerrero Terrane, *SMO* Sierra Madre Occidental, *SMOr* Sierra Madre Oriental, *SMT* Sierra Madre Terrane, *TMVB* Trans Mexican Volcanic Belt, *VSLPP* Valles-San Luis Potosí Platform

(Carrillo-Bravo 1982). The oldest record in the CMMB are Triassic low-grade metamorphic marine sedimentary rocks (Barboza-Gudiño et al. 1998, 2010; Hoppe et al. 2002), which are unconformably overlain by Lower to Middle Jurassic continental arc deposits of the Nazas Formation or "Nazas Arc" (Pantoja-Alor 1972; López-Infanzón 1986; Barboza-Gudiño et al. 1999, 2008; Bartolini et al. 2003).

Marine sedimentation throughout the Mesa Central is recorded from the Oxfordian to the end of Cretaceous. Contemporaneously, more than 4000 m thick, shallow marine carbonate sequences and clastic sediments were accumulated in the VSLPP and CMMB, covering a large portion of the central-eastern MC between the Late Triassic to Late Cretaceous (Carrillo-Bravo 1982). In addition, debris flow and turbiditic deposits are recorded between the western margin of the VSLPP and the transition towards the CMMB (Tamabra Formation; López-Doncel 2003).

The oldest rocks of the Guerrero Terrane near the study area are parts of an upper Triassic to early Jurassic accretionary subduction-related complex including quartz-rich turbidites, which locally contains blocks of chert, limestones and pillow basalts, with MORB geochemical signatures (Centeno-García et al. 1993, 2008; Martini et al. 2010; Ortega-Flores et al. 2016; Centeno-García 2017). The turbidites show zircon provenance and compositions comparable to the Triassic Potosí fan, but in contrast to them they are strongly deformed and metamorphosed (Centeno-García and Silva-Romo 1997; Centeno-García et al. 2008; Centeno-Garcia et al. 2011; Centeno-García 2017). The subduction complexes are overlain by Middle Jurassic-evolved volcanic arc rocks. Unconformably, these rocks are overlain by Early to Late Cretaceous subaerial and marine arc-related volcano-sedimentary assemblages, with greenschist facies metamorphism (Ranson et al. 1982; Freydier et al. 1996; Centeno-García and Silva-Romo 1997; Centeno-García et al. 2008).

All these Mesozoic sequences were strongly deformed during the Laramide orogeny, close to the Cretaceous–Paleogene boundary (Guzman and de Cserna 1963; Eguiluz-de Antuñano et al. 2000; Tristán-González et al. 2009b). A Paleocene–Eocene sedimentary sequence, consisting mostly of red beds or continental clastic deposits overlays the Mesozoic rocks, including intercalations of andesitic lavas that mark the first volcanic stage in central-eastern portion of the Mesa Central (49–44 Ma; Aranda-Gómez and McDowell 1998; Tristán-González et al. 2009a). This unit is followed by a more voluminous stage dominated by dacitic to rhyolitic domes, lavas, and ignimbrites (32–28 Ma; Aguillón-Robles et al. 2009; Tristán-González et al. 2009a), which are in turn overlain by mainly felsic, pyroclastic volcanic rocks, emplaced between 28 and 25 Ma, which are triggered by to the maximum extension of the Basin and Range tectonic event (Tristán-González et al. 2009b). In some volcanic centers, basaltic and andesitic lava flows are associated to the felsic volcanic rocks, showing typical characteristics of bimodal volcanism (e.g., Rodríguez-Ríos and Torres-Aguilera 2009; Tristán-González et al. 2009a; Sieck et al. 2019). Between 23 and 21 Ma, mainly fissural eruptions of basalts extruded through the faults in the southern and southwestern part of the Mesa Central are dominating. The Paleogene volcanic units are overlain by Quaternary, mainly

basanitic volcanic rocks (e.g., Labarthe-Hernández et al. 1982; Aranda-Gómez et al. 2005).

In the study area (Fig. 2), the oldest exposed rocks are Cretaceous sediments of the Cuesta del Cura Formation, a marine sequence of massive and gray limestones, interlayered with argillaceous limestones (Imlay 1936; López-Doncel 2003). The Cuesta del Cura Formation is strongly deformed and shortened due to the Laramide orogeny. Up to 250 m, Eocene–Oligocene conglomerates are interlayered with sandstones, are covering the Mesozoic marine sediments and were deposited in erosional discordance. The Mesozoic and Eocene–Oligocene sequences are overlain by the explosive rhyolitic Guanamé Ignimbrite. A K–Ar whole-rock age of 32.7 ± 1.6 Ma (Labarthe-Hernández and Jiménez-López 1991) was reported for the Guanamé Ignimbrite. Due to intense erosion, the Guanamé Ignimbrite exists as relict forming up to 30 m high ridges and plateaus aligned in N–S direction. The Oligocene volcanic activity is associated with a process of transtensive deformation, forming a set of faults with an extension of tens of kilometers, through which the magmas that originated the Oligocene volcanic rocks flowed (Tristán-González et al. 2009b). During the Pliocene–Pleistocene, sandstones that are interlayered with conglomerates, covering both, the lower Cretaceous and Oligocene volcanic rocks, were deposited in erosional discordance. This conglomerate is formed by preexisting rock clasts, consolidated to semi-consolidated in its upper part, with a thickness of 40 m. Finally, during the Quaternary, gravels and silts, caliches, lacustrine materials and alluvium were deposited.

Stratigraphy

Cuesta del Cura Formation

The oldest rocks in the studied area (Fig. 3) are a sequence of thin to medium layered, black, laminated limestones that contain layers, lenses and nodules of black chert and thin, reddish siltstone layers (Fig. 4). This sequence is called Cuesta del Cura Formation and underlies the Guanamé Ignimbrite. The Cuesta del Cura Formation represents the deepest sedimentary sequence of the Central Mexico Mesozoic Basin and based on its faunistic content (ammonites and planktonic foraminifera) it has a determined age of Albian–Turonian (Cretaceous). In thin sections, the Cuesta del Cura limestones show a groundmass of micritic matrix to microsparitic sparry cement, which nearly covers 60% of the sample, however, locally the amount of matrix/cement can vary from 30% to more than 70%. In addition, a very fine lamination, with laminae smaller than 1 mm is present and the lamination is intercalated with abundant and scarce components. The components, all smaller than 2 mm, reach percentages of between 30 and 70% and are mostly walled and unwalled calcispheres, and globular planktonic foraminifera (*Hedbergella* sp among others), similar to the examples

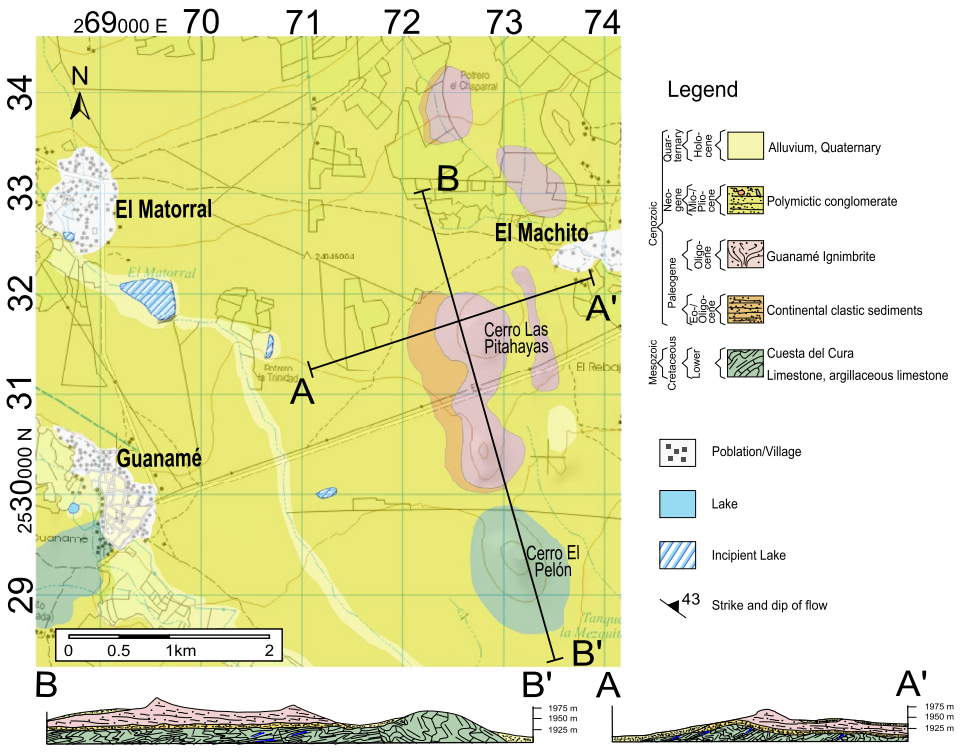

Fig. 2 Geological map of Guanamé area and cross-sections through the study area

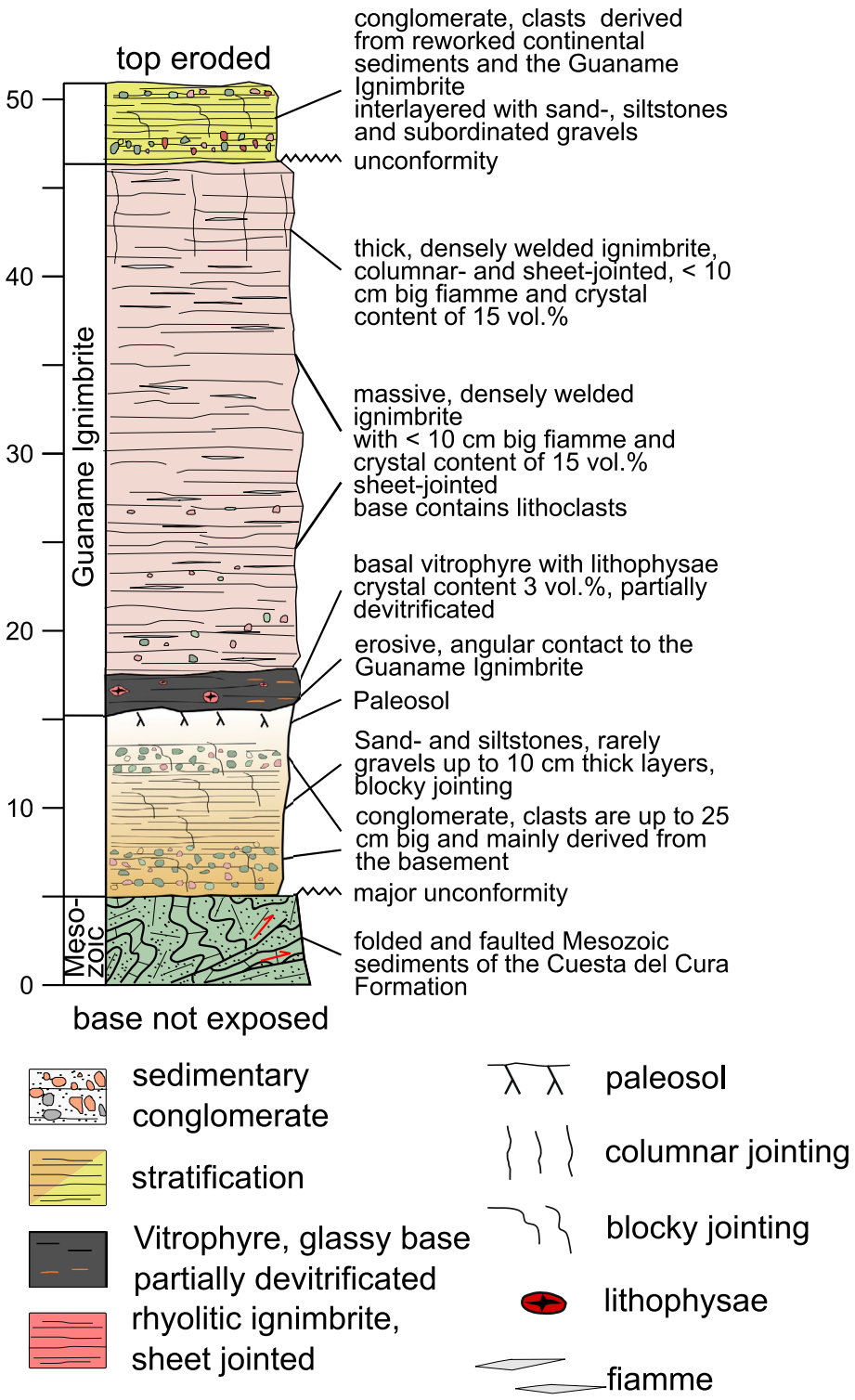

Fig. 3 Composite stratigraphic column of the Guanamé area showing the main lithostratigraphic units described in the text. Thickness given in meters

reported by Omaña et al. (2014). Small ammonites, mostly heteromorphs (*Scaphites* sp, *Baculites* sp, among others), are commonly embedded in the matrix/cement. Both, the ground mass and the percentage and type of component suggest a standard microfacies 3 (pelagic mudstone/wackestone) of a facies zone 1 (deep water basin; Wilson 1975; Flügel 2013).

Continental clastic sediments

The continental clastic sediments thickness varies from up to 200 m in basins within the folded and faulted Mesozoic rocks, to a few meters, or are not present on top of highs. The continental clastic sediments are mainly well-lithified

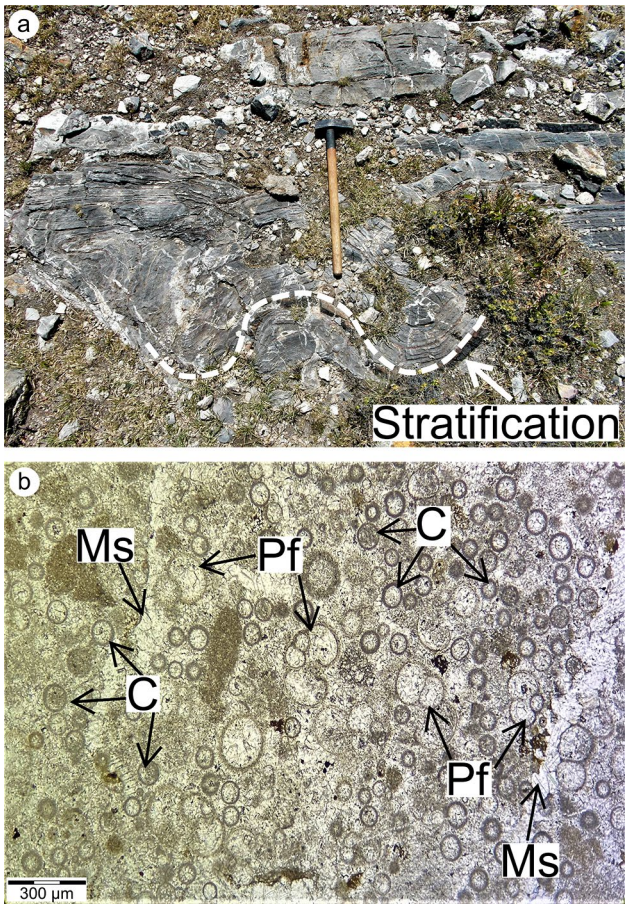

Fig. 4 **a** Folded limestones of the Cuesta del Cura formation in the study area (east of Guanamé). The dashed line retraces the stratification of the limestones. Size of the hammer is 0.5 m. **b** Thin section image of a component-rich layer of the Cuesta del Cura Formation. Pf—Pelagic foraminifer; C—Calcispheres; Ms—Microsparitic groundmass. Picture taken with parallel Nichols

conglomeratic sandstone and matrix-supported fine-grained to medium-grained polymictic conglomerate, interlayered with sand- and siltstones. Clasts in the sediments were mainly derived from the Mesozoic basement. The top sedimentary succession was eroded by the deposition of the rhyolitic Guanamé Ignimbrite.

Guanamé Ignimbrite

The Guanamé Ignimbrite forms four relictic plateaus in the eastern part of the study area (Fig. 2, Fig. 5). The base is built up by a black and crystal-rich (~20 vol.% phenocrystals; mainly sanidine, quartz, plagioclase, orthopyroxene, and biotite) basal vitrophyre that shows a low to intensive devitrification in the southern portion of the study area. Besides that, the vitrophyre contains up to 2 cm big, collapsed and elongated pumice clasts (~1 vol.%) and also, angular to sub-angular and reddish, abundant lithic components (~2 vol.% of the rock and up to 5 cm in size), mainly chert and carbonate clasts, are present. In thin sections, the basal vitrophyre can be described as seriate, holocrystalline with perlitic cracks, flow structures, as well as a low to intense devitrification (Fig. 6a). Sanidine (~10 vol.%) has an average grain size of 1.5 mm, the shape is hypidiomorphic to xenomorphic and they show Carlsbad twinning. Quartz crystals (~7 vol.%) are xenomorphic with an average grain size of 1 mm. Plagioclase crystals are less abundant (5 vol.%) and are mainly subhedral to euhedral with an average grain size of 1.5 mm. Rare biotite crystals (<1 vol.%) are also xenomorphic and have an average grain size of 0.1 mm. The orthopyroxene is intensely altered and form together with plagioclase a glomerophyric texture. Orthopyroxene are on average 0.3 mm big and have a prevalence of approximate 3 vol.%. Pumice clasts show the same mineral content, but the modal abundances are higher (quartz, 10 vol.%; sanidine, 15 vol.%; plagioclase, 10 vol.%). The vitrophyre shows no layering or graduation in grain size and turns into a pale reddish massive and densely welded porphyritic rhyolitic, up to 30 m thick and vesicle-poor ignimbrite. The Guanamé Ignimbrite is sheet jointed and in addition, the top of the unit shows columnar joints and contains sporadically up to 10 cm long and 2 cm thick fiammes. The base of the densely welded ignimbrite contains ~1 vol.% vesicles and up to 2 cm big, collapsed and elongated pumice clasts (~2 vol.%). Furthermore, the above described lithic fragments are present in all parts of the ignimbrite and are more abundant compared to the basal vitrophyre (~3 vol.%).

In thin sections, the seriate and hypocrystalline texture of the vitrophyre turns into a seriate and holocrystalline texture. The matrix of the densely welded ignimbrite consists mainly of collapsed and elongated ash and glass particles that show an increasing devitrification (Fig. 6b). Sanidine crystals (~12 vol.%) have an average grain size of 1.5 mm, the shape is hypidiomorphic to xenomorphic and they show Carlsbad twinning. Xenomorphic quartz crystals (~10 vol.%) with an average grain size of 1.0 mm and hypidiomorphic to idiomorphic and on average 2 mm big plagioclase (~7 vol.%) crystals, with polysynthetic twinning, are also present in the samples (Fig. 6 c and d). Biotite and orthopyroxene crystals show a comparable form and prevalence to the vitrophyre.

Polymictic conglomerate

A sequence of continental polymictic conglomerates that cover most parts of the study area, covers also the Guanamé Ignimbrite. The polymictic conglomerate is matrix-supported, generally fine-grained to medium-grained. Clasts in the polymictic conglomerate were derived mainly from the Guanamé Ignimbrite and the Mesozoic basement. Interlayered are the polymictic conglomerates by sand- and siltstones.

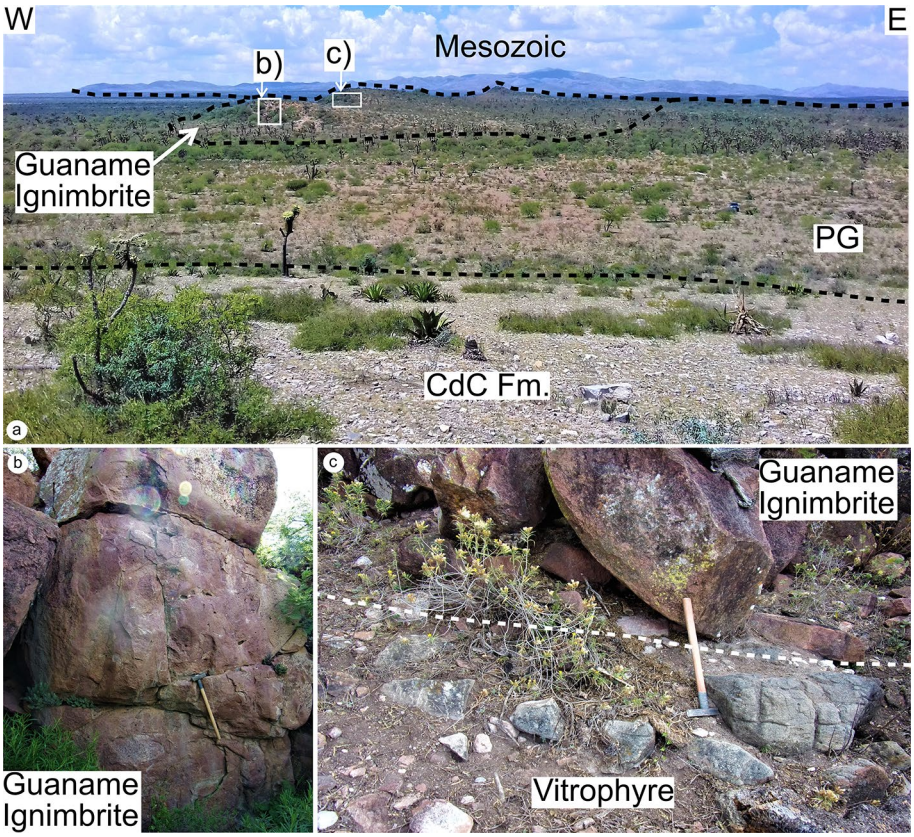

Fig. 5 Field photography from the Guanamé area. **a** Center of the study area, west of Guanamé. The dashed lines mark the geological contacts between the different geological units. CdC Fm.—Cuesta del Cura Formation. **b** Representative exposure of the densely welded Guanamé Ignimbrite in the center of the study area. Size of the hammer is 0.5 m. **c** Contact between the densely welded Guanamé Ignimbrite and its basal vitrophyre. Size of the hammer is 0.5 m

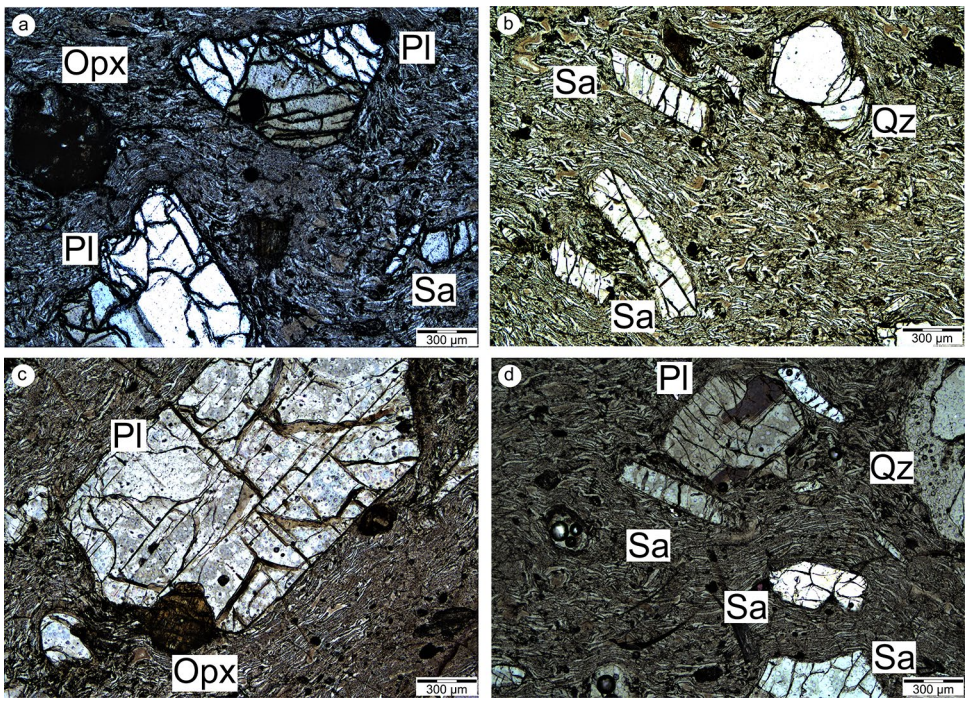

Fig. 6 Thin section images of the Guanamé Ignimbrite. **a** Plagioclase and sanidine crystals in the glassy matrix of the basal vitrophyre. Image taken with crossed nichols. **b** Sanidine and quartz crystals in the fine-grained matrix, consisting mainly of collapsed ash and glass particles. **c** Plagioclase and altered orthopyroxene crystals in the fine-grained matrix, consisting mainly of collapsed ash and glass particles. Image taken with crossed nichols. **d** Thin section image of the upper part of the Guanamé Ignimbrite, showing plagioclase, sanidine and quartz crystals. The matrix displays flow structures. Image taken with crossed nichols. Opx—orthopyroxene, Pl—plagioclase, Qz—quartz, Sa—sanidine

Analytical methods

Petrography and whole-rock geochemistry

Sample preparation was done at the Applied Geosciences Department of the IPICYT (Instituto Potosino de Investigación Científica y Tecnológica). Samples were crushed in a jaw crusher and afterwards milled in an agate planetary mono mill. Petrographic analyses were carried out on 6 samples of the Guanamé Ignimbrite. Whole-rock geochemical analyses were performed on 9 samples of Guanamé Ignimbrite. Major element analyses were done with X-ray fluorescence (RIGAKU ZSX Primus II spectrometer) at National Laboratory of Geology and Mineralogy at Geology Institute UNAM (Universidad Nacional Autónoma de México). Crushed and dried samples (0.4 g) were mixed with a mixture of $Li_2B_4O_7$ (4 g) and $LiBO_2$ (4 g) and melted down (15 min at 1100 °C) to glass tablets in platinum-gold crucibles. Matrix effect correction were calculated with the fundamental parameters method. For the analyses of major elements, the laboratory gives analytical precision better than 0.5–2 %.

The analyses of trace elements were obtained at the Geochemical Laboratory at the Geology Institute of the UASLP (Universidad Autónoma de San Luis Potosí) with a Thermo Scientific Series X2, Inductively Coupled Plasma-Quadrupole Mass Spectrometer (ICP-QMS). For the analysis, 100 mg of the powdered sample was digested with high purity degree acids of HNO_3, HF, and HCl. The detection limit of the trace-element analysis in the Geochemical Laboratory at the Geology Institute of the UASLP is reported with < 0.02 ppm, the details of the analytical method are reported by Almaguer-Rodríguez (2010).

All analyses, major and trace elements, were validated by repeated independent sample preparation, blanks, and analyses of three different international reference standards (Andesite, AGV-1, Flanagan 1967; Granodiorite, Silver Plume, Colorado, GSP-2, Wilson 1998; Quartz Latite, QLO-10, Flanagan 1976).

Mineral chemistry

Thin sections were prepared in Applied Geosciences Department, IPICYT and analyzed in the Instituto de Geofísica UNAM, Unidad Michoacán. Thin sections were polished in two steps (3 and 1 µm) and vaporized with carbon. Major elements in plagioclase and sanidine were analyzed using a JEOL JXA-8600 electron probe microanalyzer (EPMA). Analyses were made using 15 keV accelerating voltage and 10 nA beam current. The beam (spot resolution 1 µm) was focused to analyze plagioclase and sanidine. Measurements allow a spot resolution of 1–10 µm and a detection limit of < 30 ppm. All elements with an atomic number $Z \geq 5$ can be measured.

Modeling of the crystallization of the rhyolitic magmas using rhyolite-MELTS

To obtain information on the origin of the rhyolitic magmas in the Mesa Central, the rhyolite-Melts software (Gualda et al. 2012; Ghiorso and Gualda 2015) was used. Rhyolite-MELTS is a modified calibration of the original thermodynamic modeling MELTS software (Ghiorso and Sack 1995; Asimow and Ghiorso 1998). The aim in using the rhyolite-MELTS simulations is not to model in detail the crystallization of volcanic rocks in the study area, but rather to obtain important information on the range of pressure and temperature over which crystallization can take place and which minerals can crystallize from the magmas that originated the volcanic rocks in the study area. In addition, rhyolite-MELTS simulations were carried out to prove the lower crustal origin of the magmas as postulated by several authors (e.g., Aguillón-Robles et al. 2009, 2012; Sieck et al. 2019), using the geochemical data as well as pressure and temperature from crustal xenoliths of the central-eastern portion of the MC published by Schaaf et al. (1994). Two different Rhyolite-MELTS models were carried out using the geochemical composition of crustal xenoliths, the first sample is a metasediment (sample LP 51; Schaaf et al. 1994) and the second sample is a metaigneous granulite (sample LP 85; Schaaf et al. 1994). LP 51 was microscopically characterized as metasediments and consists of garnet (35%), alkali feldspar, plagioclase, sillimanite, quartz and rutile (Schaaf et al. 1994). The metaigneous granulite sample LP 85 is garnet-free and contains a mineral assemblage of plagioclase, orthopyroxene, and quartz and intermediate without any evidence of crystallization of secondary phases (Schaaf et al. 1994).

The starting pressure and temperature conditions were set as 950 °C and 8 kbar (Schaaf et al. 1994). First, fractional crystallization of the partial melt during magma ascent from the lower crust to a shallow magma chamber was modeled by decreasing the pressure (8 kbar to 2 kbar) and temperature (950 °C to 900 °C). Afterwards, equilibrium crystallization during temperature decrease (900 °C to 750 °C) in a shallow magma chamber (2 kbar) was modeled.

K–Ar whole-rock age determinations

K–Ar whole-rock ages were measured in 2 samples from Guanamé Ignimbrite in the Geoscience Center of the Georg-August-Universität Göttingen. Whole-rock samples were prepared in two different ways for argon and potassium

analysis. While the material for the determination of potassium was ground down to < 20 µm, much coarser grain size was used for the determination of argon, to avoid excessive argon losses due to comminution. The argon isotopic composition was measured in a Pyrex glass extraction and purification line coupled to a Thermo Scientific ARGUS VI™ noble gas mass spectrometer operating in static mode. The amount of radiogenic ^{40}Ar was determined by isotope dilution method using a highly enriched ^{38}Ar spike from Schumacher, Bern (Schumacher 1975). The spike is calibrated against the biotite standard HD-B1 (Fuhrmann et al. 1987). The age calculations are based on the constants recommended by the IUGS quoted in Steiger and Jäger (1977). Potassium was determined in duplicate by flame photometry using a BWB-XP flame photometer™. The samples were dissolved in a mixture of HF and HNO_3 according to the technique of Heinrichs and Herrmann (2013). The analytical error for the K/Ar age calculations is given on a 95% confidence level (2σ). Details concerning argon and potassium analyses in Göttingen laboratory are given in Wemmer (1991).

U–Pb zircon LA–ICP–MS age determinations

U–Pb zircon ages were obtained for two samples of the Guanamé Ignimbrite at the Laboratorio de Estudios Isotópicos, Centro de Geociencias, UNAM. Therefore, the samples were crushed, using a jaw crusher and the < 180 µm fraction was separated by sieving. The heavy minerals of this fraction were concentrated on a Wilfley table, the ferromagnetic portion was removed with a hand-magnet. The paramagnetic minerals were separated using a Frantz Magnetic Barrier Laboratory Separator Model LB-1 in four passes under an applied amperage of 0.3 A, 0.6 A, 0.9 A, and 1.2 A. Thereafter, a density separation with LST, a heavy liquid containing lithium heteropolytungstates in the form of extremely soluble, colorless hydrated crystals, was carried out on the non-magnetizable fraction. From the resulting heavy mineral fraction, the idiomorphic and inclusion-free zircons were manually separated using a binocular microscope. U–Pb zircon ages were obtained by laser ablation inductively coupled plasma mass spectrometry (LA–ICP–MS). For the analysis a quadrupole ICP–MS (Thermo Xii Series) was coupled to a resolution M050 excimer laser ablation workstation, using a 23-µm spot. The laboratory procedures and the laser ablation system are described by Solari et al. (2010). A detailed description of the methods and evaluation of the measurements can be found in Ortega-Obregón et al. (2014) and Solari et al. (2015). Measurements were verified using the Plešovice zircon (Sláma et al. 2008) as a bracketing standard for isotope ratios and standard glass NIST 610 to recalculate elemental concentrations.

Iolite software (Paton et al. 2010) was used for the U–Pb isotopic data reduction, age calculations and error propagations. The $^{207}Pb/^{206}Pb$ age calculations, the data visualization and common Pb correction were carried out with the VisualAge data reduction scheme for Iolite (Petrus and Kamber 2012). The calculation of concordia ages and concordia plots were performed with the Isoplot 3.0 macro for Excel (Ludwig 2003).

Results

Whole-rock geochemistry

Analytical results are shown in Table 1 and data processing and plots were carried out using GCDkit 4.1 (Janoušek et al. 2006, 2016).

The samples of the Guanamé Ignimbrite are rather fresh, with loss of ignition values (LOI at 950 °C) from 0.68 to 3.66 wt.%. The samples show a close range of

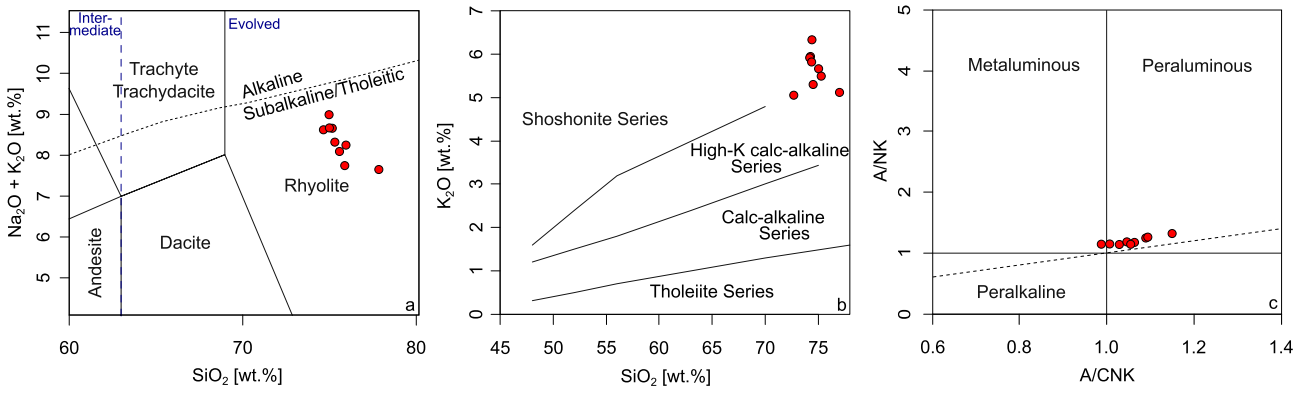

Fig. 7 Major element results for Guanamé Ignimbrite. **a** TAS classification diagram after Le Bas et al. (1986). Alkaline and subalkaline/tholeiitic fields after Miyashiro (1978). **b** K_2O vs. SiO_2 diagram after Peccerillo and Taylor (1976). **c** A/NK (molecular AL_2O_3 / $Na_2O + K_2O$) vs A/CNK (molecular Al_2O_3 /$CaO + K_2O + Na_2O$) plot after Shand (1943)

Table 1 Results of the XRF and ICP-QMS analyses

$Eu^* = \sqrt{Sm_N \times Gd_N}$ and $_N$ denotes chondrite-normalized values. Chondrite-normalized values after (McDonough and Sun 1995)

	GN-01	GN-02	GN-03	GN-04	GN-05	GN-06	GN-07	GN-08	GN-09
Major elements (wt%.)									
SiO_2	72.77	74.49	75.36	77.08	74.45	74.28	75.12	74.61	74.29
TiO_2	0.19	0.18	0.18	0.19	0.19	0.21	0.16	0.17	0.19
Al_2O_3	13.02	12.84	12.39	11.14	12.48	12.45	12.78	12.72	12.80
Fe_2O_3	1.15	2.00	1.94	1.91	2.20	2.59	2.00	2.10	2.20
MnO	0.03	0.03	0.03	0.03	0.06	0.03	0.01	0.01	0.03
MgO	0.43	0.11	0.19	0.16	0.24	0.21	0.24	0.12	0.08
CaO	0.86	0.57	0.80	0.80	0.70	1.00	0.89	0.82	0.68
Na_2O	2.97	2.58	2.69	2.45	2.75	2.65	2.37	2.31	2.64
K_2O	5.06	6.34	5.50	5.13	5.83	5.92	5.67	5.31	5.94
P2O5	0.03	0.08	0.04	0.03	0.04	0.03	0.03	0.05	0.04
LOI	3.66	0.86	0.96	1.10	1.15	0.68	0.85	2.04	1.14
Sum	100.18	100.09	100.07	100.01	100.08	100.04	100.12	100.25	100.04
Trace elements (ppm)									
Li	5.32	61.43	53.28	35.18	37.93	42.10	32.55	22.66	61.17
Sc	11.69	13.55	12.80	11.35	14.49	12.84	11.69	10.12	10.14
V	7.09	49.76	46.80	55.05	53.48	45.51	42.54	34.03	80.86
Cr	22.68	97.75	81.91	50.95	80.48	61.22	5.32	3.27	3.09
Co	0.88	2.06	2.02	1.43	2.20	1.78	0.89	1.10	0.47
Ni	10.53	51.60	43.42	24.08	41.87	30.93	2.54	1.87	1.75
Zn	45.05	45.64	45.21	42.73	48.73	43.58	46.46	42.61	39.02
Y	58.99	53.67	53.71	51.96	44.55	51.22	53.21	41.47	76.44
Zr	123.45	90.82	72.63	89.90	88.40	74.57	110.19	100.13	119.66
Nb	21.71	21.49	19.78	18.20	18.97	20.94	18.8	16.69	23.02
Rb	240.09	236.55	201.67	181.63	192.56	209.22	224.85	186.36	258.26
Sr	57.29	67.77	79.43	81.58	86.68	80.38	77.85	69.19	64.37
Cs	9.77	5.70	5.38	3.20	5.40	4.83	5.98	5.22	7.68
Ba	670.90	957.88	1125.24	960.08	1233.04	1201.33	1023.31	930.12	862.45
La	94.40	108.12	96.54	75.59	87.25	79.78	104.41	114.03	100.69
Ce	209.20	235.86	208.28	176.55	173.81	181.45	185.07	186.15	183.85
Pr	25.14	31.21	26.18	23.67	22.67	22.89	24.72	25.2	20.53
Nd	104.88	123.46	104.28	86.73	85.18	83.96	85.48	96.71	79.80
Sm	18.94	21.51	18.44	16.13	14.76	15.38	16.78	15.81	17.50
Eu	0.90	1.57	1.36	1.22	1.51	1.39	1.15	1.15	1.16
Gd	12.76	13.78	12.38	11.44	10.12	10.90	10.47	9.36	11.38
Tb	2.08	2.16	2.00	1.94	1.67	1.81	1.49	1.29	2.69
Dy	11.51	11.60	11.19	10.75	9.47	10.21	9.46	8.01	14.26
Ho	2.20	2.14	2.10	2.02	1.75	1.94	1.73	1.42	2.61
Er	6.08	5.78	5.60	5.48	5.00	5.30	4.49	3.66	7.85
Tm	0.89	0.84	0.83	0.82	0.78	0.81	0.68	0.54	1.07
Yb	5.36	5.01	4.88	4.94	4.67	4.97	4.23	3.59	6.59
Lu	0.80	0.72	0.70	0.72	0.70	0.71	0.61	0.49	0.82
Hf	4.93	3.95	3.24	4.10	4.01	3.25	4.46	4.31	3.97
Ta	1.72	1.71	1.57	1.50	1.56	1.59	1.03	0.94	1.05
Tl	3.50	1.31	1.00	0.79	0.98	1.17	1.11	0.83	0.97
Pb	32.15	34.42	30.86	28.46	29.67	30.35	27.77	27.22	26.92
Th	34.81	35.25	34.85	32.52	34.27	33.00	35.56	33.96	30.38
U	6.15	3.73	3.20	2.70	3.16	3.03	3.68	3.17	3.77
$(La/Yb)_N$	11.964	14.660	13.439	10.395	12.692	10.905	16.768	21.578	10.376
$(Eu/Eu^*)_N$	0.176	0.278	0.274	0.274	0.377	0.327	0.264	0.288	0.251

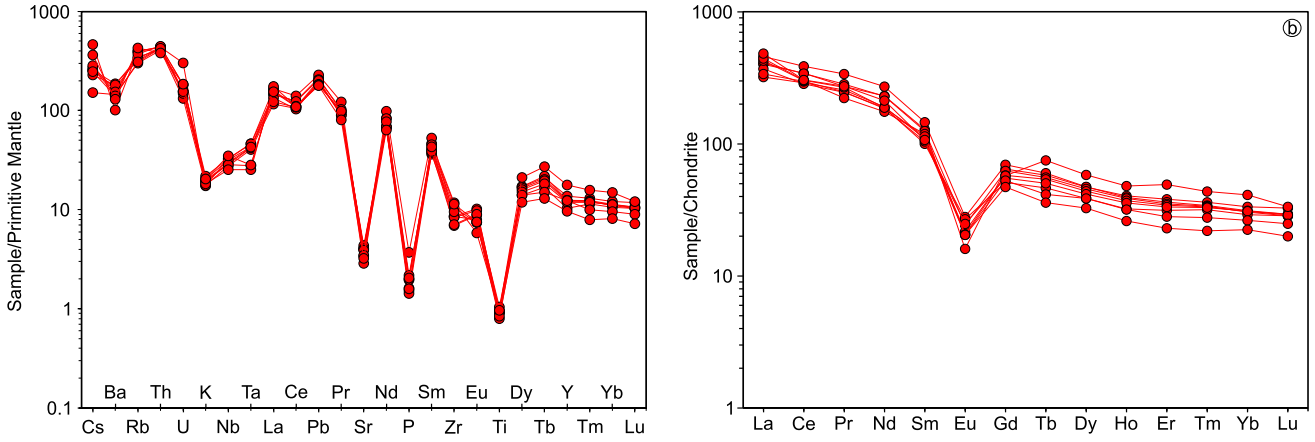

Fig. 8 **a** Primitive mantle-normalized multi-element plots and **b** chondrite-normalized rare-earth element patterns of the Guanamé Ignimbrite. Normalization values after McDonough and Sun (1995)

SiO_2 (Fig. 7a, TAS diagram) content, varying between 72.8 and 77.1 wt.%, and within this range, the sample of the vitrophyre (GN-01) has the lowest value. They are low in TiO_2 (< 0.5 wt.%) and MgO (< 0.5 wt.%). The Guanamé Ignimbrite samples correspond mostly to the high-K calc-alkaline series, with a tendency towards a shoshonitic series (Fig. 7b). Likewise, they are dominantly peraluminous, except for the sample GN-06 that is located in the metaluminous field at the boundary to the peraluminous field (Fig. 7c).

In Harker diagrams (not shown), TiO_2, Fe_{total}, MgO, MnO, and Na_2O display negative correlations with SiO_2, whereas K_2O and CaO show positive correlations. The concentrations of incompatible elements increase with increasing SiO_2, whereas the compatible elements decrease with increasing SiO_2 content.

Trace element patterns in the primitive mantle-normalized multi-element plots (Fig. 8a) display a general negative slope, with marked negative anomalies of Ba, Nb, Ta, Sr, P, and Ti and weak positive anomalies of Th, Pb, and a general enrichment in large ion lithophile elements (LILE) concerning to high field strength elements (HFSE). On the other hand, chondrite-normalized REE patterns (Fig. 8b) show an enrichment in LREE compared to HREE ($10.38 \leq (La/Yb)_N \leq 21.58$; $_N$ denotes chondrite-normalized values, Table 1) and compared to the LREE, the HREE patterns are sub-horizontal. Total REE abundances range from 418.00 to 563.76 ppm. A slightly to well-developed Eu anomaly is present in all samples of the Guanamé Ignimbrite (Fig. 8b) with $(Eu/Eu^*)_N$ between 0.18 and 0.38 ($Eu^* = \sqrt{Sm_N \times Gd_N}$, Table 1).

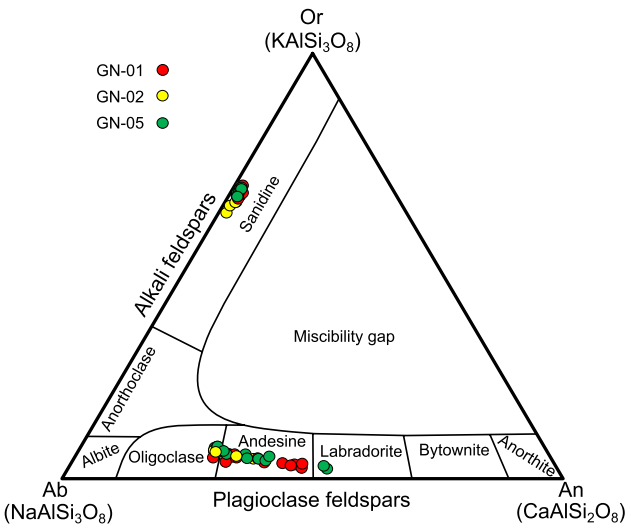

Fig. 9 Ternary classification of feldspars from the Guanamé Ignimbrite

Mineral chemistry

EPMA were performed to determine the end-member composition of plagioclase and K-feldspar of three samples of the Guanamé Ignimbrite (Appendix). The results of the EPMA are summarized in Fig. 9. All alkali feldspars of the sample from the base of the ignimbrite (GN-01) are sanidine, with an orthoclase content ranging between 62.54 and 68.80 wt.%. The analyzed plagioclase crystals from the base of the ignimbrite are mainly andesine and subordinated oligoclase (An = 27.02–35.85 wt.%). The composition of alkali feldspars from the central part of the ignimbrite (GN-02) is comparable to the base of the ignimbrite. All of the analyzed alkali feldspars are sanidine, with an orthoclase content ranging between 65.87 and 68.96 wt.%. Plagioclase are mainly andesine and oligoclase (An = 27.26–46.54 wt.%). The alkali feldspar from the top of the Guanamé Ignimbrite

(GN-05) are sanidine (Or = 66.36–68.49 wt.%) and the plagioclase composition are mainly andesine and subordinated oligoclase (An = 26.83–38.73 wt.%). Two plagioclase show a labradorite composition (An = 50.70 wt.% and 51.73 wt.%).

Rhyolite-MELTS crystallization models

The initial mineral assemblages and the amounts of partial melt generated at 8 kbar and 950 °C from the metasediment and the metaigneous granulite are shown in Table 2.

The mineral assemblage and mineral composition are the same for all investigated initial total water contents (0.1, 0.2 and 0.3 wt.% H_2O) and are comparable to the description of Schaaf et al. (1994). With an increasing water in the system, the modeled mineral assemblage of the metasediment sample LP 51 shows a nearly constant garnet content, whereas the amount of the other minerals decrease. In contrast, the modeled composition of the metaigneous granulite sample LP 85 shows a nearly constant pyroxene content, whereas all other minerals, decrease with increasing water content (Table 2).

In Fig. 10, the results of the rhyolite-MELTS crystallization models are summarized and all models result in a mineral assemblage similar to the observed mineral composition of the Guanamé Ignimbrite. The water content directly controls the quantity of generated partial melt from the lower crustal xenoliths, as well as the water content in the partial melt. In addition, the water content in the partial melt controls the crystallization temperatures of the different mineral phases (Fig. 10, Appendix). The crystallization temperature of quartz, orthopyroxene, and biotite from the modeled partial melt increases with increasing water content (Fig. 10), whereas, the crystallization temperatures of K-feldspar are oppositional for the partial melts of the metasediments. With increasing crystallization temperature of quartz, the crystallization temperature of K-feldspar decreases. In the metaigneous granulites, the crystallization temperature of K-feldspar and quartz decrease with increasing water content. The models show that orthopyroxene become unstable and dissolve with decreasing temperature and biotite starts to crystallize.

Plagioclase crystals that crystallize from the partial melt of the metasediment (LP51) show a similar composition to the plagioclases from the Guanamé Ignimbrite (Fig. 11). In contrast, the plagioclases derived from the metaigneous granulite (LP 85) are richer in Ca compared to the Guanamé Ignimbrite but become richer in Na with increasing initial water content. Both, the modeled sanidine that crystallize from the partial melt of the metasediments and the partial melt of the metaigneous granulites are enriched in K compared to the sanidine from the Guanamé Ignimbrite analyzed in this study.

Geochronology

Cathodoluminescence (CL) images of the zircons indicate that most of the zircons are characterized by oscillatory magmatic zoning with U-rich (dark zones/colors in CL images; Fig. 12a) and U-poor (bright zones/colors in CL images) zones. In general, the zircons are euhedral and elongated to short prismatic with width to length ratios ranging from 1:1 to 1:6. The weighted mean U–Pb ages and the corresponding intercept ages are reported with mean square of weighted deviates (MWSD) and 2 sigma errors, where both, the random and the systematic errors were considered. Uncertainties in the U–Pb data are reported with 2 sigma error in the Appendix.

The zircons of the sample GN-07 have all low concentrations in U and Pb, resulting in discordant data points. The Discordia intersects the Concordia at 30.6 ± 0.7 Ma (n = 34, MWSD = 1.5; Fig. 12b). The Th/U ratios for the analyzed zircons of the sample GN-07 range from 0.37 to 1.07.

The analyses of the zircons of the sample GN-08 yielded a weighted mean $^{206}Pb/^{238}U$ age of 30.7 ± 0.4 Ma (n = 12, MWSD = 5.67; Fig. 12c, d). The Th/U ratios for the analyzed zircons of the sample GN-08 range from 0.40 to 1.14. Compared to the sample GN-07, the zircons of the sample GN-08 are mostly concordant.

Table 2 Initial conditions of rhyolite-MELTS models for the samples LP 51 and LP 85 from Schaaf et al. (1994). RHM-oxides summarize rutile, hematite, and magnetite

Sample	LP 51 0.1 wt.% H_2O	LP 51 0.2 wt.% H_2O	LP 51 0.3 wt.% H_2O	LP 85 0.1 wt.% H_2O	LP 85 0.2 wt.% H_2O	LP 85 0.3 wt.% H_2O
Mineral phases (wt.%)						
Melt	7.00	10.58	13.71	8.54	12.68	15.97
Garnet	25.84	25.92	25.89	–	–	–
Plagioclase	26.99	24.76	22.91	44.46	43.28	41.59
Quartz	37.83	36.56	35.42	18.63	17.48	16.14
RHM-oxide	2.13	2.03	1.96	1.94	1.86	1.77
Apatite	0.10	0.07	0.03	0.08	0.05	0.01
Orthopyroxene	–	–	–	24.19	24.56	24.43

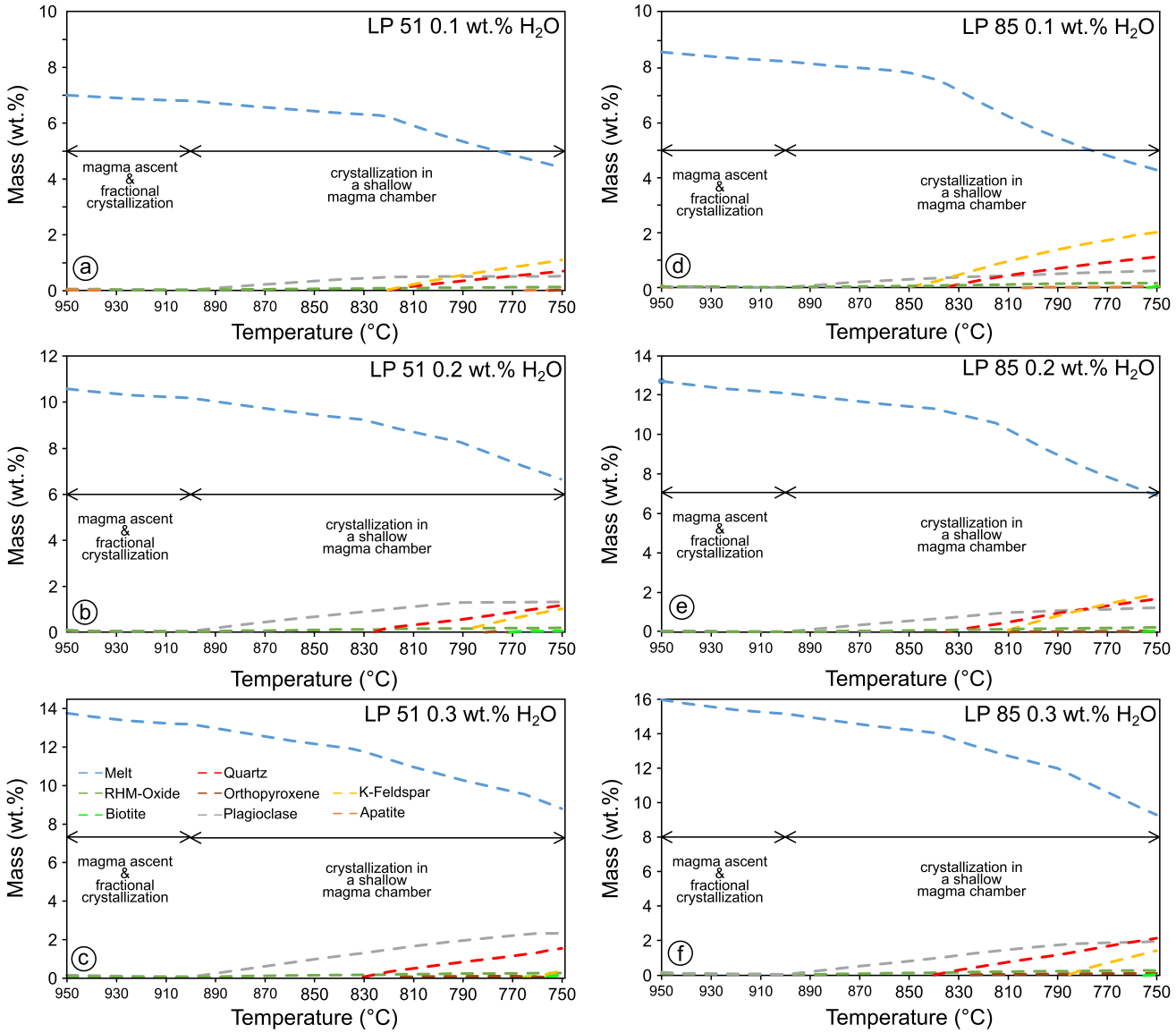

Fig. 10 Rhyolite-MELTS fractional crystallization and equilibrium crystallization models for partial melt of lower crustal metasediments and metaigneous granulites from the Mexican state of San Luis Potosí. Data for the samples LP 51 and LP 85 are derived from Schaaf et al. (1994). **a** Crystallization model of the partial melt of sample LP 51 containing an initial content of 0.1 wt.% H_2O. **b** Crystallization model of the partial melt of sample LP 51 containing an initial content of 0.2 wt.% H_2O. **c** Crystallization model of the partial melt of sample LP 51 containing an initial content of 0.3 wt.% H_2O. **d** Crystallization model of the partial melt of sample LP 85 containing an initial content of 0.1 wt.% H_2O. **e** Crystallization model of the partial melt of sample LP 85 containing an initial content of 0.2 wt.% H_2O. **f** Crystallization model of the partial melt of sample LP 85 containing an initial content of 0.3 wt.% H_2O

Results of the K–Ar whole-rock age determinations are shown in Table 3. Two ages of 30.1 ± 0.5 Ma (GN-01) and 30.7 ± 0.9 Ma (GN-02) were obtained for the Guanamé Ignimbrite. The determined ages are younger than the reported K–Ar whole-rock age of 32.7 ± 1.6 Ma from Labarthe-Hernández and Jiménez-López (1991).

The analysis of the sample GN-02 has only 33.57% radiogenic argon (Ar*), possibly because of Ar loss, 67% is air contamination and had to be corrected, hence the error for GN-02 is bigger. Therefore, the result of the sample GN-01 is analytically more credible.

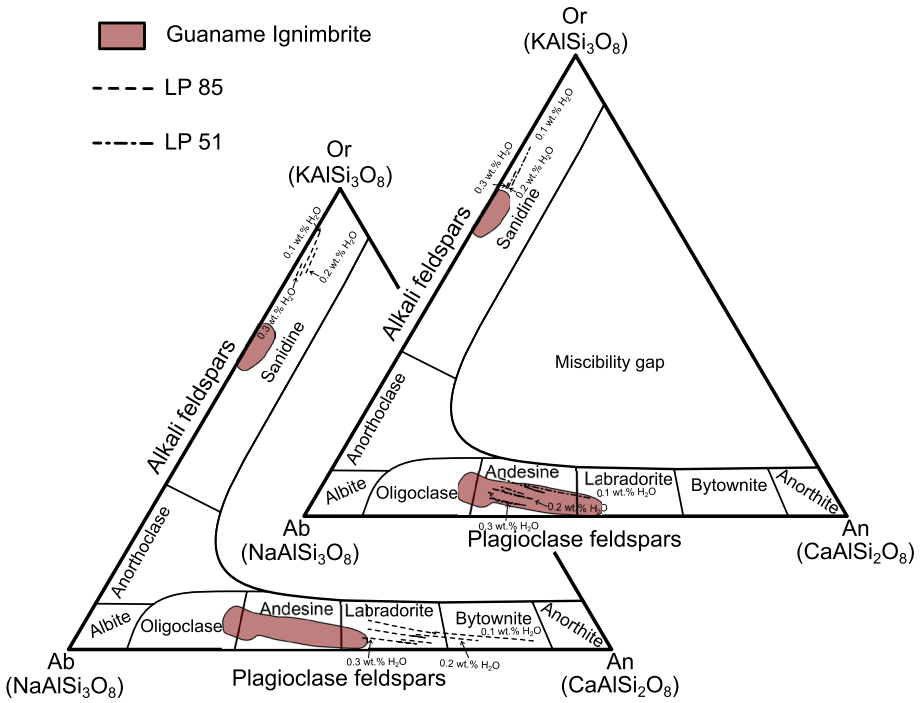

Fig. 11 Feldspar classification diagram for the feldspars from the Guanamé Ignimbrite analyzed in this work and the results of the rhyolite-MELTS crystallization models

Discussion

Genesis of the Guanamé Ignimbrite

The lower crustal origin of the rhyolitic magmas that originated the rhyolitic ignimbrites and domes is still under debate. Aguillón-Robles et al. (2009) proposed for the Oligocene rhyolitic domes in the southern MC a model including partial melting of the lower continental crust, direct ascent through the brittle crust and eruption. Newer investigations on the Oligocene garnet-bearing rhyolites of La Herradura (Fig. 1c) show that the almandine-rich garnets crystallized at lower crustal depth from a rhyolitic magma (Sieck et al. 2019).

The Guanamé Ignimbrite is a typical rhyolitic ignimbrite with a geochemistry comparable to rhyolitic ignimbrites and rhyolitic lava flows and domes in the center and western portion of the Mesa Central (Aguillón-Robles et al. 2009, 2012, 2014; Sieck et al. 2019; Torres-Sánchez et al. 2019). The eruption age of the Guanamé Ignimbrite is younger than the ages of the El Sombrero Ignimbrite and La Herradura Rhyolite from the La Herradura area (K–Ar whole-rock age, 33.3 ± 0.43 Ma and 31.25 ± 0.7 Ma; Sieck et al. 2019; Fig. 1c) and all are older than the Panalillo Ignimbrite (K–Ar whole-rock age, 28.84 ± 0.71 Ma, 1σ; Tual 2010) in the southern portion of the SVRVF (Fig. 1c). The eruption ages derived from the Santa Maria Ignimbrite in the Rio Santa Maria volcanic field (K–Ar whole-rock ages between 32.8 ± 0.5 and 31.3 ± 0.7 Ma, 1 σ; Tristán-González et al. 2009a; Fig. 1c) and in the Villa Hidalgo volcanic complex (K–Ar whole-rock ages between 31.7 ± 0.7 and 31.0 ± 0.7 Ma, 1 σ; Tristán-González et al. 2009a) as well as the Cantera Ignimbrite in the Sierra San Miguelito volcanic complex (ages between 29.0 ± 1.5 Ma, 1 σ, K–Ar whole rock; Labarthe-Hernández et al. 1982; U–Pb zircon ages 30.14 ± 0.16 Ma and 30.62 ± 0.23 Ma, 2 σ; Del Pilar-Martínez et al. 2020) indicate a contemporaneous emplacement of the ignimbrites in the Mesa Central. As in other volcanic units from the central portion of the Mesa Central, for example in the La Herradura area (Sieck et al. 2019), the U–Pb crystallization ages of zircons (30.7 ± 0.4 Ma and 30.6 ± 0.7 Ma) and the K–Ar whole-rock ages (30.1 ± 0.5 Ma and 30.68 ± 0.94 Ma) overlap, indicating a short time between partial melt of the source and eruption of the rhyolitic volcanic rocks in the Mesa Central. These ages coincide with the Oligocene peak of the SMO silicic large igneous province where at least a volume of 300,000 km^3 (75% of the total volume of volcanic rocks in the SMO) was extruded (Ferrari et al. 2007, 2018; Bryan and Ernst 2008; Tristán-González et al. 2009b). Most of the erupted volume (85–90%) is represented by rhyolitic ignimbrites, such as the Guanamé Ignimbrite, and the remaining by rhyolitic lavas, domes as well as basaltic and andesitic lavas (Bryan and Ferrari 2013; Ferrari et al. 2018).

The high content of SiO_2 together with the low content of MgO, Cr, and Ni indicate an evolved magma. In addition, all but one sample are peraluminous, pointing out a saturation in Al_2O_3, and affiliation to a high-K calc-alkaline to shoshonitic series with ferroan character. This is related to the generation and evolution of magmas under

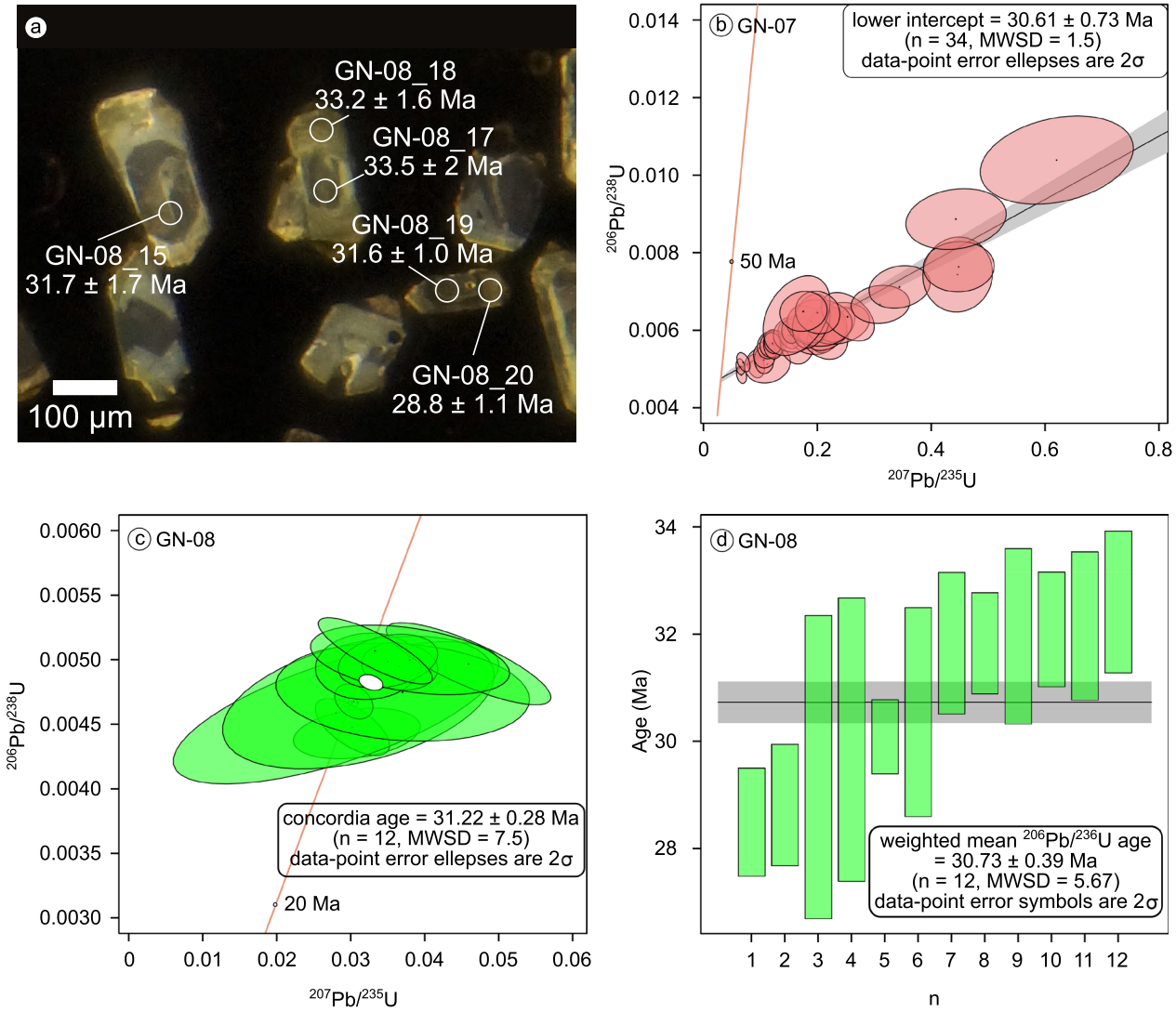

Fig. 12 Results of the U–Pb zircon age dating. **a** Cathodoluminescence images of representative zircons with individual $^{206}Pb/^{238}U$ ages and respective 2σ errors (sample GN-08) **b** Discordia of the analyzed zircons from the sample GN-07 intersects with the concordia at 30.61 ± 0.73 Ma. **c** Concordia diagram of the zircons from the sample GN-08. **d** Weighted mean age plots for the concordant U–Pb zircon age determinations. Green colors signify concordant ages and red signify discordant

Table 3 Results of the K–Ar whole-rock age determinations

Sample	Unit	Spike [No.]	K_2O [Wt. %]	40 Ar * [nl/g] STP	40 Ar * [%]	Age [Ma]	2σ-error [Ma]	2σ-error [%]
GN-01	Guanamé Ignimbrite	5967	4.62	4.52	78.69	30.12	0.45	1.5
GN-02	Guanamé Ignimbrite	5969	5.80	5.79	33.57	30.68	0.94	3.1

reducing conditions, leading to iron enrichment (Frost and Frost 2008). In the multi-element plots (Fig. 8), large ion lithophile elements such as Rb, Th, and U are enriched and Nb, Ta and the feldspar compatible elements Ba, Sr and Eu show negative anomalies. Enrichment of incompatible elements and depletion of compatible elements show that fractionation during the generation of these rocks took place, possibly in a magma chamber prior to eruption and/or during the ascent of the magma. The negative anomalies of the feldspar compatible elements (Ba, K, and Sr; Fig. 8), as

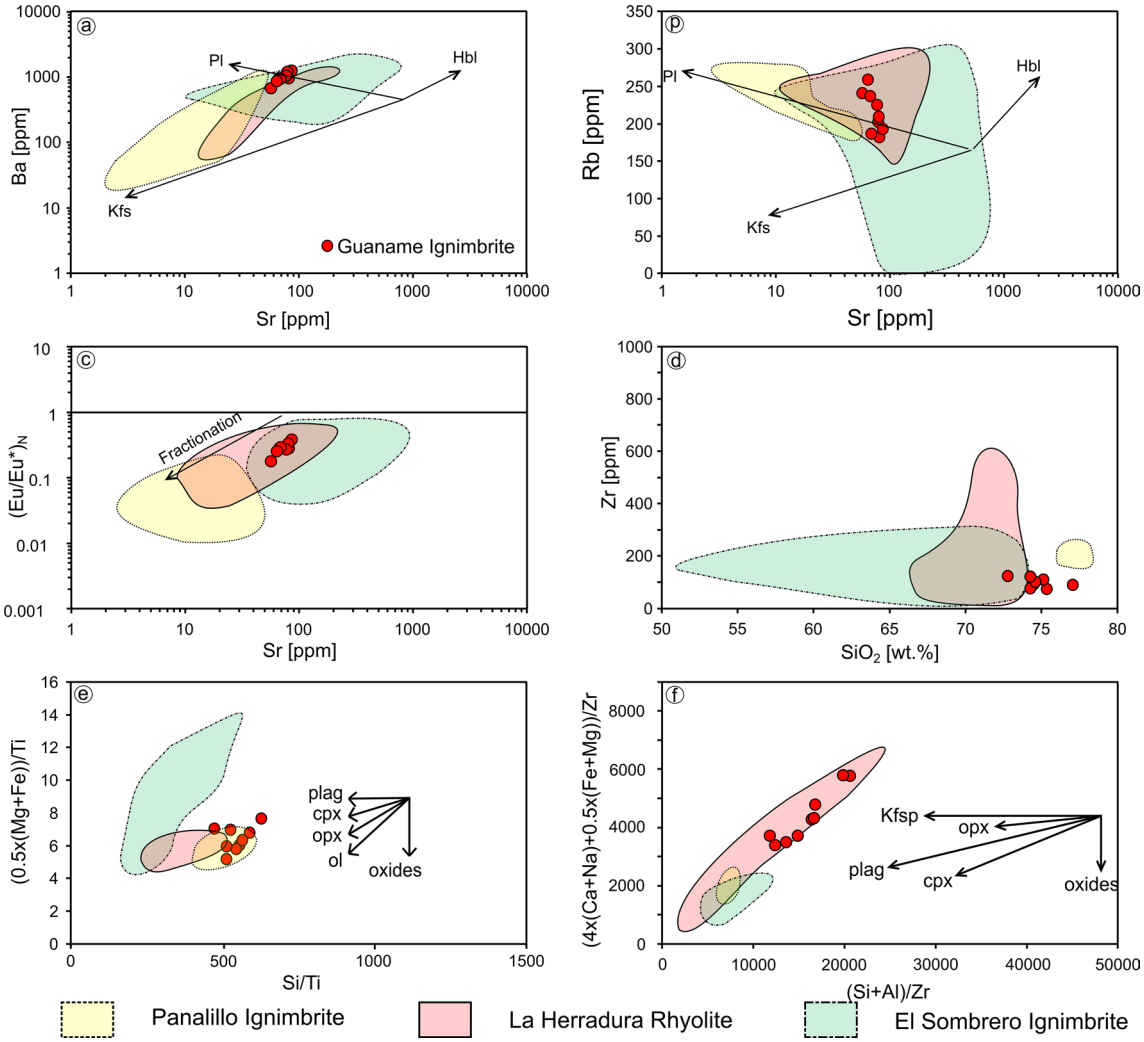

Fig. 13 Co-variations of element concentrations and elemental ratios diagrams of the volcanic rocks of the Guanamé Ignimbrite. **a** Ba vs. Sr; **b** Rb vs. Sr; **c** Eu/Eu* vs. Sr; **d** Zr vs. SiO_2. **e** and **f** Pearce Element ratio diagrams (after Pearce 1968; Pearce and Cann 1973; Bradshaw 1992) showing crystal fractionation trends for the Guanamé Ignimbrite and the volcanic rocks from the SVRVF. Data of the volcanic rocks from the SVRVF taken from Rodríguez-León (2012) and Sieck et al. (2019)

well as the correlations between Rb and Ba with Sr indicate that plagioclase was the main fractionating phase during the evolution of these magmas (Fig. 13). The fractional crystallization is confirmed in the change of the composition of K-feldspar and plagioclase in the different samples from the Guanamé Ignimbrite (Fig. 9). The concentrations of zirconium in the Guanamé Ignimbrite are quite variable, but low (< 150 ppm) and not correlated to the SiO_2 concentration of the rocks (Fig. 13). Rhyolite-Melts crystallization models with the composition, pressure and temperature conditions of lower crustal metasediments and metaigneous granulites (Schaaf et al. 1994) show that depending on the initial water content (0.1, 0.2, and 0.3 wt.% H_2O), ~ 7 to ~ 16 wt.% partial melt can be generated. The initial water concentrations to generate the partial melting are low. It is well known that water is released by the dehydration of hydrous mineral during metamorphism (e.g., Reverdatto et al., 2019). In addition, the extensional setting during the Oligocene (e.g., Tristán-González et al. 2009b) might have favored the partial melting of the lower crust due to decompression. The initial mineral assemblage (Table 2) in the models is similar to the sample description reported in Schaaf et al. (1994). During the ascent of the partial melt fractional crystallization was applied in the rhyolite-MELTS models, resulting in the fractional crystallization of mainly plagioclase and oxides, confirming the geochemical results presented in this study (Fig. 8; Fig. 13). The modeled crystallization of the ascended magma in a shallow magma chamber (2 kbar) resulted in the same mineral assemblage as observed in the samples of the Guanamé Ignimbrite. In thin sections, all the orthopyroxene crystals are altered, whereas the other mineral phases are not affected by intense alteration pointing

out that the orthopyroxene was not in equilibrium in the magma chamber (Fig. 6) and biotite is only observed as small crystals (≥ 150 µm) in the vitrophyre. The observation is confirmed by the rhyolite-MELTS models, orthopyroxene become unstable at lower temperatures and biotite crystallization initiates.

The mineral composition of plagioclases analyzed in this study ranges between labradorite and oligoclase (An = 26.83–51.73 wt.%) and all K-feldspars are sanidine with orthoclase contents between 62.54 and 68.96 wt.%. The composition of the plagioclases of the rhyolite-MELTS models is comparable to the results presented in this study; nevertheless, the orthoclase-composition of the sanidine is slightly different (Fig. 11). The difference in composition might be the result of the assimilation of upper crustal material during the ascent and storage of the magma. Three sections from sanidine to plagioclase were analyzed to calculate the crystallization temperature of the feldspars (Appendix), using the Eq. 27b in Putirka (2008). The calculated crystallization temperatures of feldspar are between 805 ± 30 and 838 ± 35 °C, matching the K-feldspar crystallization temperatures of the rhyolite-MELTS models (Fig. 10). The trace-element behavior in the multi-element plots (Fig. 8) implies that the rhyolitic volcanic rocks were the result of a process involving partial melting of the lower crust and fractional crystallization. Based mainly on the behavior of Nb and Ta, the rhyolitic magma of the Guanamé Ignimbrite is produced in an intra-plate setting and confirmed by the bi-element variation diagrams shown in Fig. 14. If the magma source was subduction related, these elements should be more depleted due to differentiation (Gill 2012). Nevertheless, all samples plot in the TAS diagram (Fig. 7) in the subalkaline field, which is on the contrary of the intra-plate setting. The samples show a clear tendency to the alkaline field and the subalkaline character might be inherited from the lower crustal xenoliths that originated the rhyolitic magmas. The enrichment of the LREE decreases, whereas the HREE patterns are almost horizontal, those patterns are indicating intra-plate signatures, whereas strong negative patterns are typical for subduction-related magmas (Wilson 2007). Besides, the negative anomalies of the trace elements Ba, Th and Nb indicate a generation of the rhyolitic magmas in the lower crust (Fig. 14).

In comparison to the other volcanic units in the Salinas-Villa de Ramos volcanic field (SVRVF) (Figs. 1, 13, and 14), the rhyolitic Guanamé Ignimbrite show similarities to the El Sombrero Ignimbrite, the garnet-bearing La Herradura rhyolite, and the Panalillo Ignimbrite. In addition, the Guanamé Ignimbrite shows similar trace-element and REE patterns as the San Miguelito Rhyolite of the Pinos volcanic complex south of the study area (Tristán-González et al. 2008, 2009a) and the same fractionation trends as the other volcanic rocks from the SVRVF (Fig. 13). The geochemical results show a similar process of formation and evolution as the El Sombrero Ignimbrite, the Panalillo Ignimbrite and the La Herradura Rhyolite, but in contrast to the La Herradura Rhyolite, the Guanamé Ignimbrite is the product of a major explosive eruption, following temporary storage in a shallow magma chamber, in which volatiles were exsolved. Such ignimbrite-generating events occurred in many areas of the Mesa Central and the adjacent Sierra Madre Occidental (Aguirre-Díaz and Labarthe-Hernández 2003; Aguirre-Díaz et al. 2008; Ferrari et al. 2018).

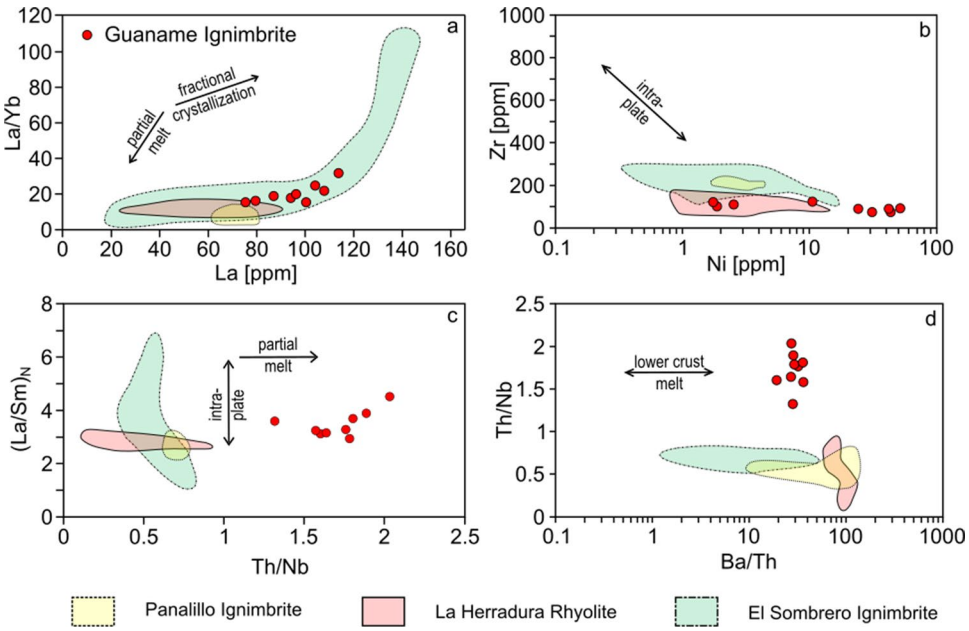

Fig. 14 Bi-element variation diagrams for samples of the Guanamé Ignimbrite and the volcanic rocks from the SVRVF. **a** $[La/Sm]_N$ vs. Th/Nb; $_N$ denotes chondrite-normalized values after McDonough and Sun (1995). **b** Zr vs. Ni. **c** La/Yb vs. La. **d** Th/Nb vs. Ba/Th. Data of the volcanic rocks from the SVRVF taken from Rodríguez-León (2012) and Sieck et al. (2019)

Geodynamic implications of the eruption and emplacement of the rhyolitic ignimbrites

The formation of the SMO and its southeastern portion, the MC, includes three main tectono-volcanic stages, during which most of the volcanic rocks in the southern and central portion of the Mesa Central were emplaced in the Eocene, Oligocene and Miocene (e.g., Labarthe-Hernández et al. 1982; Aranda-Gómez and McDowell 1998; Nieto-Samaniego et al. 2007; Aguillón-Robles et al. 2009; Tristán-González et al. 2009a). The Eocene igneous pulse is characterized by volcanism of andesitic composition that occurred at 45–42 Ma and 36–34 Ma (Aguillón-Robles et al. 2009; Tristán-González et al. 2009a). The second phase of volcanic activity in the Mesa Central overlaps in space and time with the main phase of volcanic activity of the Sierra Madre Occidental (Nieto-Samaniego et al. 2007; Tristán-González et al. 2009b; Ferrari et al. 2018). As in the SMO, the Oligocene to Miocene igneous event can be distinguished in two pulses: first, an Oligocene (~32–28 Ma) and second, an early Miocene (~24–20 Ma) pulse, both consisting of mainly rhyolitic volcanic rocks, and subordinate rhyodacite and dacite (e.g., Labarthe-Hernández et al. 1982; Nieto-Samaniego et al. 2007; Tristán-González et al. 2009a). The third event corresponds to an extension-related Miocene mafic volcanism that has been related to the evolution from a continental arc regime to intra-plate volcanism including subalkaline andesites and alkaline basalts (e.g., Aguirre-Díaz and McDowell 1993; Nieto-Samaniego et al. 2007; Tristán-González et al. 2009a; Aguillón-Robles et al. 2014). In the SMO and in its southeastern portion, the MC, calderas are not evident for most ignimbrites (Aguirre-Díaz and Labarthe-Hernández 2003; Nieto-Samaniego et al. 2007; Aguirre-Díaz et al. 2008; Tristán-González et al. 2009a). The Guanamé area shows no evidences of a caldera or caldera-like structures. Aguirre-Díaz and Labarthe-Hernández (2003) presented a field-based model for fissure-fed ignimbrite eruptions and graben calderas mainly based on their observations of pyroclastic dykes in grabens all over the MC. The Oligocene felsic magmatism overlaps in time with an intense phase of the extensional tectonics of the Basin and Range, extending in NNW–SSE direction. This favored the ascent of the rhyolitic magmas through the brittle crust documented in explosive (ignimbrite flare-up) as well as effusive (lava flows and domes) and fissure-type eruptions all over the MC (Aguirre-Díaz and Labarthe-Hernández 2003; Aguirre-Díaz et al. 2008; Tristán-González et al. 2008; Aguillón-Robles et al. 2009, 2014; Rodríguez-Ríos and Torres-Aguilera 2009; Sieck et al. 2021). Regional geological and geophysical studies imply that in the southern and central part of the Mesa Central the crust has a thickness of approximately 30–33 km, whereas the thickness of the crust to the west is 40–42 km and to the east 37 km (e.g., Fix 1975; Nieto-Samaniego et al. 2007). The thinning of the crust in this part was apparently due to the extension of the Basin and Range province during the Oligocene to Miocene (e.g., Tristán-González et al. 2009b). These may have favored the generation of the acidic magmas, due to decompression, and the ascent of the rhyolitic magmas in the SVRVF and all over the MC (e.g., Aguillón-Robles et al. 2009; Tristán-González et al. 2009b; Sieck et al. 2019). This results in the alignment of the rhyolitic domes (e.g., garnet-bearing La Herradura Rhyolite; Sieck et al. 2019 and southern MC; Aguillón-Robles et al. 2009) and the eruption of rhyolitic ignimbrites along NNW-SSE trending major faults (e.g., Oligocene rhyolitic Ignimbrites in the SLPVF; Torres-Hernández et al. 2006). The Guanamé Ignimbrite might be the result of a fissure-fed eruption and the eruption ages of the Guanamé Ignimbrite coincide with a major extensional phase in the Mesa Central (Tristán-González et al. 2009b). Nevertheless, there are no pyroclastic dikes exposed in and near the study area, but they might be covered by Neogene and Quaternary sediments.

Conclusions

The present work shows the geochemical, petrological and geochronological evolution of the Oligocene rhyolitic volcanism in the central and eastern portion of the Mesa Central of Mexico based on the example of the Guanamé Ignimbrite. The results show that the high-K calc-alkaline to shoshonitic and high-silica rhyolitic magmas of the study area are derived from a complex process including the partial melting of the lower crust in an intra-plate extensional setting during an intense phase of the Basin and Range extension. The geochronological analyses indicate a crystallization of zircons from the rhyolitic magmas between 30.61 ± 0.73 and 30.73 ± 0.39 Ma (zircon single grain U–Pb ages) and an eruption age of 30.12 ± 0.45 Ma (K–Ar whole-rock age). Chondrite-normalized rare-earth element patterns show enrichment of the LREE compared to the HREE and negative Eu anomaly and flat shape for HREE. The primitive mantle-normalized diagram shows an enrichment in incompatible elements with negative anomalies in Nb, Ta, Ti, Ba, Sr, and P. Change of mineral composition, mainly in K-feldspar and plagioclase, in combination with the trace and REE patterns show that during the ascent and storage of the rhyolitic magmas, fractional crystallization of mainly plagioclase and oxides was the main process taking place during the evolution of these magmas. Geochemical features and mineral chemistry prove the lower crustal origin of the rhyolitic magmas by partial melting in an intra-plate and extensional setting.

Geothermal constraints on the crystallization temperatures of feldspar and mineral chemistry of feldspars show

similar temperatures and compositions as the rhyolite-MELTS crystallization models. The models reveal that these rhyolitic magmas were generated by partial melting of the well-studied lower crust in the MC and also, they result in a mineral assemblage similar to the Guanamé Ignimbrite and similar ignimbrites in the central and eastern portion of the MC.

Supplementary Information The online version contains supplementary material available at https://doi.org/10.1007/s00531-021-02088-8.

Acknowledgements The authors want to thank Erasmo Mata Martínez from the UASLP and María Mercedes Zavala Arriaga from IPICYT for assistance with sample preparation. The authors also wish to thank Miguel Ángel Cortina Rangel for ICP–MS sample preparation and analytical data. The first author thanks for the financial support of the National Council of Science and Technology, Mexico (CONACYT) through Ph.D. scholarship number 590738. The rock age determinations were done thanks to the financial support of agreement C19-FAI-05-05.50 of the second author. Furthermore, the authors would like to thank the reviewers Dr. Peter Schaaf and Dr. Luigi Solari for their comments on the review of this article that helped to improve our hypothesis.

References

Aguillón-Robles A, Aranda-Gómez JJ, Solorio-Munguía JG (1994) Geología y tectónica de un conjunto de domos riolíticos del Oligoceno Medio en el sur del Estado de San Luis Potosí, México. Revista Mexicana De Ciencias Geológicas 11:29–42

Aguillón-Robles A, Tristán-González M, Aguirre-Díaz GJ, Bellon H (2009) Syn-extensional intra-plate trachydacite-rhyolitic dome volcanism of the Mesa Central, southern Sierra Madre Occidental volcanic province, Mexico. J Volcanol Geoth Res 187:33–52. https://doi.org/10.1016/j.jvolgeores.2009.08.021

Aguillón-Robles A, Tristán-González M, López-Doncel RA, García-Arreola ME, Almaguer-Rodríguez JdL, Maury RC (2012) Trace elements geochemistry and origin of volcanic units from the San Luis Potosí and Río Santa María volcanic fields, Mexico: the bearing of ICP-QMS data. Geofísica Internacional 51:293–308

Aguillón-Robles A, Tristán-González M, Aguirre-Díaz GJ, López-Doncel RA, Bellon H, Martínez-Esparza G (2014) Eocene to Quaternary mafic-intermediate volcanism in San Luis Potosí, central Mexico: the transition from Farallon plate subduction to intra-plate continental magmatism. J Volcanol Geoth Res 276:152–172. https://doi.org/10.1016/j.jvolgeores.2014.02.019

Aguirre-Díaz GJ, Labarthe-Hernández G, Tristán-González M, Nieto-Obregón J, Gutiérrez-Palomares I (2008). Chapter 4 The Ignimbrite Flare-Up and Graben Calderas of the Sierra Madre Occidental, Mexico. In: Gottsmann J, Martí J (eds) Caldera Volcanism: Analysis, Modelling and Response. Developments in Volcanology 10, pp 143–180

Aguirre-Díaz GJ, Labarthe-Hernández G (2003) Fissure ignimbrites: Fissure-source origin for voluminous ignimbrites of the Sierra Madre Occidental and its relationship with Basin and Range faulting. J Geophys Res 31:773–776. https://doi.org/10.1130/G19665.1

Aguirre-Díaz GJ, McDowell FW (1991) The volcanic section at Nazas, Durango, Mexico, and the possibility of widespread Eocene volcanism within the Sierra Madre Occidental. J Geophys Res 96:13373–13388. https://doi.org/10.1029/91JB00245

Aguirre-Díaz GJ, McDowell FW (1993) Nature and timing of faulting and synextensional magmatism in the southern Basin and Range, central-eastern Durango, Mexico. Geol Soc Am Bull 105:1435–1444. https://doi.org/10.1130/0016-7606(1993)105%3c1435:NATOFA%3e2.3.CO;2

Almaguer-Rodríguez JdL (2010) Estudio geoquímico de elementos traza en unidades volcánicas del CVSLP: método ICP–MS (validación del método). Tesis Ingeniería Geológica: Universidad Autónoma de San Luis Potosí, Facultad de Ingeniería

Aranda-Gómez JJ, McDowell FW (1998) Paleogene extension in the Southern Basin and Range Province of Mexico: syndepositional tilting of eocene red beds and oligocene volcanic rocks in the Guanajuato Mining District. Int Geol Rev 40:116–134. https://doi.org/10.1080/00206819809465201

Aranda-Gómez JJ, Luhr JF, Housh TB, Valdez-Moreno G, Chávez-Cabello G (2005) El volcanismo tipo intraplaca del Cenozoico tardío en el centro y norte de México: una revisión. Boletín De La Sociedad Geológica Mexicana 57:187–225

Aranda-Gómez JJ, Molina-Garza R, McDowell FW, Vassallo-Morales LF, Ortega-Rivera MA, Solorio-Munguía JG, Aguillón-Robles A (2007) The relationships between volcanism and extension in the Mesa Central: the case of Pinos, Zacatecas, Mexico. Revista Mexicana De Ciencias Geológicas 24:216–233

Asimow PD, Ghiorso MS (1998) Algorithmic modifications extending MELTS to calculate subsolidus phase relations. Am Miner 83:1127–1132

Barboza-Gudiño JR, Tristán-González M, Torres-Hernández JR (1998) The Late Triassic-Early Jurassic active continental margin of western North America in northeastern Mexico. Geofísica Internacional 37:283–292

Barboza-Gudiño JR, Orozco-Esquivel MT, Gómez-Anguiano M, Zavala-Monsiváis A (2008) The Early Mesozoic volcanic arc of western North America in northeastern Mexico. J S Am Earth Sci 25:49–63. https://doi.org/10.1016/j.jsames.2007.08.003

Barboza-Gudiño JR, Zavala-Monsiváis A, Venegas-Rodríguez G, Barajas-Nigoche LD (2010) Late Triassic stratigraphy and facies from northeastern Mexico: Tectonic setting and provenance. Geosphere 6:621–640. https://doi.org/10.1130/GES00545.1

Barboza-Gudiño JR, Tristán-González M, Torres-Hernández JR (1999) Tectonic setting of pre-Oxfordian units from central and northeastern Mexico: A review. In: Bartolini C, Wilson JL, Lawton TF (eds) Mesozoic sedimentary and tectonic history of north-central Mexico. Geological Society of America Special Paper 340, pp 197–210

Bartolini C, Lang H, Spell T. (2003) Geochronology, geochemistry, and tectonic setting of the Mesozoic Nazas arc in north-central Mexico, and its continuation to northern South America. In: Bartolini C, Buffler RT, Blickwede JF (eds) The Circum-Gulf of Mexico and the Caribbean: Hydrocarbon Habitats, Basin Formation, and Plate Tectonics. American Association of Petroleum Geologists Memoir vol. 79, pp 427–461

Bradshaw TK (1992) The adaptation of Pearce element ratio diagrams to complex high silica systems. Contrib Mineral Petrol 109:450–458

Bryan SE, Ernst RE (2008) Revised definition of Large Igneous Provinces (LIPs). Earth Sci Rev 86:175–202. https://doi.org/10.1016/j.earscirev.2007.08.008

Bryan SE, Ferrari L (2013) Large igneous provinces and silicic large igneous provinces: Progress in our understanding over the last 25 years. J Geophys Res 125:1053–1078. https://doi.org/10.1130/B30820.1

Bryan SE, Ferrari L, Reiners PW, Allen CM, Petrone CM, Ramos-Rosique A, Campbell IH (2008) New insights into crustal contributions to large-volume rhyolite generation in the Mid-Tertiary Sierra Madre Occidental Province, Mexico, Revealed by U-Pb

Geochronology. J Petrol 49:47–77. https://doi.org/10.1093/petrology/egm070
Cameron KL, Hanson GN (1982) Rare earth element evidence concerning the origin of voluminous mid-Tertiary rhyolitic ignimbrites and related volcanic rocks, Sierra Madre Occidental, Chihuahua, Mexico. Geochim Cosmochim Acta 46:1489–1503. https://doi.org/10.1016/0016-7037(82)90309-X
Campa MF, Coney PJ (1983) Tectono-stratigraphic terranes and mineral resource distributions in Mexico. Can J Earth Sci 20:1040–1051. https://doi.org/10.1139/e83-094
Carrillo-Bravo J (1982) Exploración petrolera de la Cuenca Mesozoica del Centro de México. Boletín De La Asociación Mexicana De Geólogos Petroleros 34:21–46
Centeno-García E (2017) Mesozoic tectono-magmatic evolution of Mexico: an overview. Ore Geol Rev 81:1035–1052. https://doi.org/10.1016/j.oregeorev.2016.10.010
Centeno-García E, Silva-Romo G (1997) Petrogenesis and tectonic evolution of central Mexico during Triassic-Jurassic time. Revista De La Mexicana De Ciencias Geológicas 14:244–260
Centeno-García E, Ruíz J, Coney PJ, Patchett PJ, Ortega-Gutiérrez F (1993) Guerrero terrane of Mexico: its role in the Southern, Cordillera from new geochemical data. Geol 21:419–422. https://doi.org/10.1130/0091-7613(1993)021%3c0419:GTOMIR%3e2.3.CO;2
Centeno-Garcia E, Busby C, Busby M, Gehrels G (2011) Evolution of the Guerrero composite terrane along the Mexican margin, from extensional fringing arc to contractional continental arc. Geol Soc Am Bull 123:1776–1797. https://doi.org/10.1130/B30057.1
Centeno-García E, Guerrero-Suastegui M, Talavera-Mendoza O (2008) The Guerrero Composite Terrane of western Mexico: Collision and subsequent rifting in a supra-subduction zone. In: Draut A, Clift PD, Scholl DW (eds) Formation and Applications of the Sedimentary Record in Arc Collision Zones. Geological Society of America Special Paper 436, pp 279–308
Del Pilar-Martínez A, Nieto-Samaniego AF, Alaniz-Alvarez SA, Angeles-Moreno E (2020) Geology of the southern Mesa Central of Mexico: recording the beginning of a polymodal fault system. J Maps 16:199–211. https://doi.org/10.1080/17445647.2020.1719911
Eguiluz-de Antuñano S, Aranda-García M, Marrett R (2000) Tectónica de la Sierra Madre Oriental, México. Boletín De La Sociedad Geológica Mexicana 53:1–26
Ferrari L, Orozco-Esquivel T, Bryan SE, López-Martínez M, Silva-Fragoso A (2018) Cenozoic magmatism and extension in western Mexico: linking the Sierra Madre Occidental silicic large igneous province and the Comondú Group with the Gulf of California rift. Earth Sci Rev 183:115–152. https://doi.org/10.1016/j.earscirev.2017.04.006
Ferrari L, López-Martínez M, Rosas-Elguera J (2002) Ignimbrite flare-up and deformation in the southern Sierra Madre Occidental, western Mexico: Implications for the late subduction history of the Farallon plate. Tectonics 21:17-1–17-24. https://doi.org/10.1029/2001TC001302
Ferrari L, Valencia-Moreno M, Bryan S (2007) Magmatism and tectonics of the Sierra Madre Occidental and its relation with the evolution of the western margin of North America. In: Alaniz-Álvarez SA, Nieto-Samaniego ÁF (eds) Geology of México: Celebrating the Centenary of the Geological Society of México. Geological Society of America Special Paper 422, pp 1–39
Fix JE (1975) The Crust and Upper Mantle of Central Mexico. Geophys J Int 43:453–499. https://doi.org/10.1111/j.1365-246X.1975.tb00643.x
Flanagan FJ (1967) U.S. Geological Survey silicate rock standards. Geochim Cosmochim Acta 31:289–308
Flanagan FJ (1976) Descriptions and analyses of eight new USGS Rock standards, U.S. Geological Survey Professional Paper 840:1–192
Flügel E (2013) Microfacies of carbonate rocks: analysis, interpretation and application. Springer Science & Business Media
Freydier C, Martinez JR, Lapierre H, Tardy M, Coulon C (1996) The Early Cretaceous Arperos oceanic basin (western Mexico). Geochemical evidence for an aseismic ridge formed near a spreading center. Tectonophysics 259:343–367. https://doi.org/10.1016/0040-1951(95)00143-3
Frost BR, Frost CD (2008) A Geochemical Classification for Feldspathic Igneous Rocks. J Petrol 49:1955–1969. https://doi.org/10.1093/petrology/egn054
Fuhrmann U, Lippolt HJ, Hess JC (1987) Examination of some proposed K-Ar standards: analyses and conventional K-Ar data. Chem Geol 66:41–51. https://doi.org/10.1016/0168-9622(87)90027-3
Ghiorso MS, Gualda GAR (2015) An H2O–CO2 mixed fluid saturation model compatible with rhyolite-MELTS. Contrib Mineral Petrol 169:1–30. https://doi.org/10.1007/s00410-015-1141-8
Ghiorso MS, Sack RO (1995) Chemical mass transfer in magmatic processes IV. A revised and internally consistent thermodynamic model for the interpolation and extrapolation of liquid-solid equilibria in magmatic systems at elevated temperatures and pressures. Contrib Mineral Petrol 119:197–212
Gill JB (2012) Orogenic andesites and plate tectonics. Springer Science & Business Media.
González-Naranjo GA, Molina-Garza RS, Aranda-Gómez JJ, Tristán-González M, Aguillón-Róbles A, Iriondo A, Bellón H (2012) Paleomagnetismo y edad de la Ignimbrita Panalillo Superior, Campo Volcánico de San Luis Potosí, México. Boletín De La Sociedad Geológica Mexicana 64:387–409
Gualda GAR, Ghiorso MS, Lemons RV, Carley TL (2012) Rhyolite-MELTS: a modified calibration of MELTS optimized for silica-rich, fluid-bearing magmatic systems. J Petrol 53:875–890. https://doi.org/10.1093/petrology/egr080
Guzman EJ, de Cserna Z (1963) Tectonic history of Mexico. In: Childs OE, Beebe BW (eds) Backbone of the Americas: Tectonic History from Pole to Pole. American Association of Petroleum Geologists Memoir vol. 2, pp 113–129
Heinrichs H, Herrmann AG (2013) Praktikum der analytischen Geochemie. Springer-Verlag
Hoppe M, Barboza-Gudiño JR, Schulz HM (2002) Late Triassic submarine fan deposits in northwestern San Luis Potosí, Mexico—lithology, facies and diagenesis. Neues Jahrbuch für Geologie und Paläontologie—Monatshefte 12:705–724. https://doi.org/10.1127/njgpm/2002/2002/705
Imlay RW (1936) Part IV. Geology of the western part of the Sierra de Parras. Geol Soc Am Bull 47:1091–1152
Janoušek V, Farrow CM, Erban V (2006) Interpretation of whole-rock geochemical data in igneous geochemistry: introducing geochemical data toolkit (GCDkit). J Petrol 47:1255–1259
Janoušek V, Moyen JF, Martin H, Erban V, Farrow C (2016) Geochemical modelling of igneous processes—principles and recipes in R language. Springer, Berlin Heidelberg, Berlin, Heidelberg
Labarthe-Hernández G, Jiménez-López LS (1991) Cartografía geológica 1: 50000 de las hojas Cerritos de Bernal, Santo Domingo, El Estribo y La Herradura, estado de San Luis Potosí. Instituto de Geología y Metalurgia, Universidad Autónoma de San Luis Potosí, Foll Téc 113
Labarthe-Hernández G, Tristán-González M, Aranda-Gómez JJ (1982) Revisión estratigráfica del Cenozoico de la parte central del Estado de San Luis Potosí. Instituto de Geología y Metalurgia, Universidad Autónoma de San Luis Potosí, Foll Téc 85
Le Bas MJ, Le Maitre RW, Streckeisen A, Zanettin B (1986) A chemical classification of volcanic rocks based on the total alkali-silica diagram. J Petrol 27:745–750
López-Doncel RA (2003) La Formación Tamabra del Cretácico medio en la porción central del margen occidental de la

Plataforma Valles-San Luis Potosí, centro-noreste de México. Revista Mexicana De Ciencias Geológicas 20:1–19
López-Infanzón M (1986) Estudio petrogenético de las rocas ígneas en las Formaciones Huizachal y Nazas. Boletín De La Sociedad Geológica Mexicana 47:1–41
Ludwig KR (2003) Isoplot 3.00, a geochronological toolkit for microsoft excel. Berkeley Geochronology Center, Berkeley
Martini M, Ferrari L, López-Martínez M, Valencia V (2010) Stratigraphic redefinition of the Zihuatanejo area, southwestern Mexico. Revista Mexicana De Ciencias Geológicas 27:412–430
McDonough WF, Sun S-S (1995) The composition of the Earth. Chem Geol 120:223–253. https://doi.org/10.1016/0009-2541(94)00140-4
McDowell FW, Clabaugh SE (1979) Ignimbrites of the Sierra Madre Occidental and their relation to the tectonic history of western Mexico. Geol Soc Am Spec Pap 180:113–124
Miyashiro A (1978) Nature of alkalic volcanic rock series. Contrib Mineral Petrol 66:91–104
Nieto-Samaniego ÁF, Alaniz-Álvarez SA, Camprubí A (2007) Mesa Central of México: Stratigraphy, structure, and Cenozoic tectonic evolution. In: Alaniz-Álvarez SA, Nieto-Samaniego ÁF (eds) Geology of México: celebrating the centenary of the geological society of México. Geological Society of America Special Paper 422, pp 41–70
Omaña L, Torres JR, López-Doncel R, Alencáster G, López-Caballero I (2014) A pithonellid bloom in the Cenomanian-Turonian boundary interval from Cerritos in the western Valles-San Luis Potosí platform, Mexico: Paleoenvironmental significance. Revista Mexicana De Ciencias Geológicas 31:28–44
Orozco-Esquivel MT, Nieto-Samaniego AF, Alaniz-Alvarez SA (2002) Origin of rhyolitic lavas in the Mesa Central, Mexico, by crustal melting related to extension. J Volcanol Geoth Res 118:37–56. https://doi.org/10.1016/S0377-0273(02)00249-4
Ortega-Flores B, Solari LA, Escalona-Alcázar FD (2016) The Mesozoic successions of western Sierra de Zacatecas, Central Mexico: provenance and tectonic implications. Geol Mag 153:696–717. https://doi.org/10.1017/S0016756815000977
Ortega-Obregón C, Solari L, Gómez-Tuena A, Elías-Herrera M, Ortega-Gutiérrez F, Macías-Romo C (2014) Permian-Carboniferous arc magmatism in southern Mexico: U-Pb dating, trace element and Hf isotopic evidence on zircons of earliest subduction beneath the western margin of Gondwana. Int J Earth Sci (geol Rundsch) 103:1287–1300. https://doi.org/10.1007/s00531-013-0933-1
Pantoja-Alor J (1972) La Formación Nazas del Levantamiento de Villa Juárez, Estado de Durango. Memorias de la Segunda Convención Nacional de la Sociedad Geológica Mexicana 25–31.
Paton C, Woodhead JD, Hellstrom JC, Hergt JM, Greig A, Maas R (2010) Improved laser ablation U-Pb zircon geochronology through robust downhole fractionation correction. Geochem Geophys Geosyst 11:1–36. https://doi.org/10.1029/2009GC002618
Pearce TH (1968) A contribution to the theory of variation diagrams. Contrib Mineral Petrol 19:142–157
Pearce JA, Cann JR (1973) Tectonic setting of basic volcanic rocks determined using trace element analyses. Earth Planet Sci Lett 19:290–300
Peccerillo A, Taylor SR (1976) Geochemistry of eocene calc-alkaline volcanic rocks from the Kastamonu area, Northern Turkey. Contrib Mineral Petrol 58:63–81. https://doi.org/10.1007/BF00384745
Petrus JA, Kamber BS (2012) VizualAge: a novel approach to laser ablation ICP–MS U–Pb geochronology data reduction. Geostand Geoanal Res 36:247–270. https://doi.org/10.1111/j.1751-908X.2012.00158.x
Putirka KD (2008) Thermometers and barometers for volcanic systems. Rev Mineral Geochem 69:61–120. https://doi.org/10.2138/rmg.2008.69.3
Ranson WA, Fernández LA, Simmons WB Jr, de la Vega SE (1982) Petrology of the metamorphic rocks of Zacatecas, Zac., Mexico. Boletín De La Sociedad Geológica Mexicana 43:37–59
Reverdatto VV, Likhanov II, Polyansky OP, Sheplev VS, Kolobov VY (2019) The nature and models of metamorphism. Springer International Publishing
Rodríguez-León L (2012) Evolución geológica del Campo Volcánico Salinas-Villa de Ramos. Tesis de Maestría, Universidad Autónoma de San Luis Potosí, Instituto de Geología San Luis Potosí
Rodríguez-Ríos R, Torres-Aguilera JM (2009) Evolución petrológica y geoquímica del vulcanismo bimodal oligocénico en el campo volcánico de San Luis Potosí (México). Revista Mexicana De Ciencias Geológicas 26:658–673
Schaaf P, Heinrich W, Besch T (1994) Composition and Sm-Nd isotopic data of the lower crust beneath San Luis Potosí, central Mexico: evidence from a granulite-facies xenolith suite. Chem Geol 118:63–84
Schumacher E (1975) Herstellung von 99, 9997% 38Ar für die 40K/40Ar Geochronologie. Geochronologia Chimia 24:441–442
Shand SJ (1943) Eruptive rocks: their genesis, composition, classification, and their relation to ore-deposits, with a chapter on meteorites. Wiley, New York
Sieck P, López-Doncel R, Dávila-Harris P, Aguillón-Robles A, Wemmer K, Maury RC (2019) Almandine garnet-bearing rhyolites associated to bimodal volcanism in the Mesa Central of Mexico: geochemical, petrological and geochronological evolution. J S Am Earth Sci 92:310–328. https://doi.org/10.1016/j.jsames.2019.03.018
Sieck P, Dávila-Harris P, López-Doncel RA, Almaguer J, Aguillón-Robles A, Wemmer K, Guevara R (2021) Voluminous Paleogene volcanism in the southern Mesa Central, Mexico: Unravelling the fissure-fed origin of rhyolitic ignimbrites of the Villa Garcia-Loreto Volcanic Complex. J Volcanol Geothermal Res 107252. https://doi.org/10.1016/j.jvolgeores.2021.107252
Sláma J, Košler J, Condon DJ, Crowley JL, Gerdes A, Hanchar JM, Horstwood MSA, Morris GA, Nasdala L, Norberg N, Schaltegger U, Schoene B, Tubrett MN, Whitehouse MJ (2008) Plešovice zircon—a new natural reference material for U-Pb and Hf isotopic microanalysis. Chem Geol 249:1–35. https://doi.org/10.1016/j.chemgeo.2007.11.005
Smith RD, Cameron KL, McDowell FW, Niemeyer S, Sampson DE (1996) Generation of voluminous silicic magmas and formation of mid-Cenozoic crust beneath north-central Mexico: evidence from ignimbrites, associated lavas, deep crustal granulites, and mantle pyroxenites. Contrib Miner Petrol 123:375–389. https://doi.org/10.1007/s004100050163
Solari LA, Gómez-Tuena A, Bernal JP, Pérez-Arvizu O, Tanner M (2010) U-Pb zircon geochronology with an integrated LA–ICP–MS microanalytical workstation: achievements in precision and accuracy. Geostand Geoanal Res 34:5–18. https://doi.org/10.1111/j.1751-908X.2009.00027.x
Solari LA, Ortega-Obregón C, Bernal JP (2015) U-Pb zircon geochronology by LAICPMS combined with thermal annealing: achievements in precision and accuracy on dating standard and unknown samples. Chem Geol 414:109–123. https://doi.org/10.1016/j.chemgeo.2015.09.008
Steiger RH, Jäger E (1977) Subcommission on geochronology: convention on the use of decay constants in geo- and cosmochronology. Earth Planet Sci Lett 36:359–362. https://doi.org/10.1016/0012-821X(77)90060-7

Swanson ER, McDowell FW (1984) Calderas of the Sierra Madre Occidental volcanic field western Mexico. J Geophys Res 89:8787–8799. https://doi.org/10.1029/JB089iB10p08787

Torres-Hernández JR, Labarthe-Hernández G, Aguillón-Robles A, Gómez-Anguiano M, Mata-Segura JL (2006) The pyroclastic dikes of the Tertiary San Luis Potosí volcanic field: implications on the emplacement of Panalillo ignimbrite. Geofísica Internacional 45:243–253

Torres-Sánchez D, Verma SK, Verma SP, Velasco-Tapia F, Torres-Hernández JR (2019) Petrogenetic and tectonic implications of Oligocene−Miocene volcanic rocks from the Sierra de San Miguelito complex, central Mexico. J S Am Earth Sci 95:102311. https://doi.org/10.1016/j.jsames.2019.102311

Tristán-González M, Labarthe-Hernández G, Aguirre-Díaz GJ, Aguillón-Robles A (2008) Tectono-volcanic control of fissure type vents for the 28 Ma Panalillo ignimbrite in the Villa de Reyes Graben, San Luis Potosí, México. IOP Conf Ser 3:12026. https://doi.org/10.1088/1755-1307/3/1/012026

Tristán-González M, Aguillón-Robles A, Barboza-Gudiño JR, Torres-Hernández JR, Bellon H, López-Doncel R, Rodríguez-Ríos R, Labarthe-Hernández G (2009a) Geocronología y distribución espacial del vulcanismo en el Campo Volcánico de San Luis Potosí. Boletín De La Sociedad Geológica Mexicana 61:287–303

Tristán-González M, Aguirre-Díaz GJ, Labarthe-Hernández G, Torres-Hernández JR, Bellon H (2009b) Post-Laramide and pre-Basin and Range deformation and implications for Paleogene (55–25 Ma) volcanism in central Mexico: a geological basis for a volcano-tectonic stress model. Tectonophysics 471:136–152. https://doi.org/10.1016/j.tecto.2008.12.021

Tual T (2010) Trace elements geochemistry and origin of volcanic units from the San Luis Potosi and Rio Santa Maria volcanic fields, Mexico: the bearing of ICP-QMS data. Mémoire de stage de Master 2, Université de Bretagne Occidentale

Verma SP (1984) Sr and Nd isotopic evidence for petrogenesis of mid-tertiary felsic volcanism in the mineral district of Zacatecas, Zac. (Sierra Madre Occidental). Mexico Chem Geol 46:37–53. https://doi.org/10.1016/0009-2541(84)90164-5

Wemmer K (1991) K/Ar-Altersdatierungsmöglichkeiten für retrograde Deformationsprozesse im spröden und duktilen Bereich-Beispiele aus der KTB-Vorbohrung (Oberpfalz) und dem Bereich der Insubrischen Linie (N-Italien). Göttinger Arbeiten Zur Geologie Und Paläontologie 51:1–61

Wilson JL (1975) Carbonate facies in geologic history. Springer, Berlin

Wilson SA (1998) Data compilation for USGS reference material GSP-2, Granodiorite, Silver Plume, Colorado, U.S. Geological Survey Open-File Report

Wilson BM (2007) Igneous petrogenesis a global tectonic approach. Springer Science & Business Media